THE UNIVERSITY F READING

DEPARTMENT F MATHEMATICS

Higher Order Balance Conditions Using Hamiltonian Dynamics for Numerical Weather Prediction

y Steven James Fletcher

Dissertation submitted for the degree of

Doctor of Philosophy

Feb 2004

ontenten

hapter 1

Introduction

The problem with data assimilation is the sparseness of observations of the atmosphere over certain areas of the Earth, mainly the oceans, does not provide initial conditions at the required operational resolution. This problem is overcome by using information about the atmospheric movements prior to the data assimilation and this requires the evaluation of the balanced and unbalanced parts of the flow. The decomposition is often referred to as a *control variable transform.*

Currently at the Met Office this decomposition is achieved by transforming the wind field, $\mathbf{u}$, into its rotational part, (relative vorticity), ξ, and divergent part, δ. From these there are two elliptic partial

represents the semi-geostrophic part of the equations. Associated with this phase space is a set of canonical coordinates which turned out to be those derived by Hoskins in [21]. These coordinates have special features and have been used operationally, [15], but the semi-geostrophic equations are also seen as an important part of research in numerical weather modelling, [13], [45], [47] and [52].

McIntyre and Roulstone in [30] and [31] are able to extend the ideas derived by Salmon and are able to derive a relationship between the sub-space, (they refer to it as a constrained submanifold) and the canonical coordinates. The potential vorticity associated with the manifolds can be written as a Monge-Ampère equation between the canonical coordinates and the Lagrangian fluid particle coordinates.

If we consider the vertical component of the relative vorticity of the balanced wind field then this is related to the depth of the fluid by a Monge-Ampère equation for a balanced height. From this height we calculate the balanced wind field. This field is not divergence free, but is balanced as it defines the sub-space of the shallow water equations that does not excite the fast waves.

In this thesis we investigate this new wind field as a possible alternative for the current decomposition to rotational and divergent fields in the control variable transform. We start in Chapter 2 where we briefly introduce the

tions to the elliptic equations, and compare these results with those from the constant coefficient equations to see if there is any extra information coming from the extra terms. We also perform a scale analysis at 72 hrs on the terms in the differential equation for the same reason.

The reason for these experiments is that the new equation requires a nine-point stencil to approximate it rather than the five-point for the Laplacian and as such if the Laplacian is the dominant term then it may not be economical to calculate the extra terms involving the variable coefficients. We also perform a scale analysis of the terms in the ellipticity conditions at 72 hrs to see if there are any terms that could be removed from the equations.

The second set of experiments involve the numerical solutions of the new elliptic equations where we consider, as a first choice, a zonal averaged base state and we examine the effects that this has when considered with the three test cases. We also test to see if the result about using the PV with a low Burger number flow regime, [57], carries over to the higher form of the PV that we derive in Chapter 4. W

cedure to derive an initialisation that prevents the fast motions forming in the numerical solution. The result is a choice between two sets of conditions. The first is a set of initial conditions and the second is a Monge-Ampère equation that is referred to as a ***non-linear balance equation*** whose solution does not include the fast waves.

.1 Atmospheric Motions

We begin with a quote from a letter that appears in [14] from Jule Charney to Phillip Thompson. Charney has the following description for the atmosphere:

" *We might say that the atmosphere is a musical instrument on which one can play many tunes. High notes are the sound waves, low notes are long inertial waves, and nature is a musician more of the Beethoven than of the Chopin type. He much prefers the low notes and only occasionally plays arpeggios in the treble and then only with a light hand. The oceans and the continents are the elephants in Saint-Saens' animal suite, marching in a slow cumbrous rhythm, one step every day or so. f course, there are overtones; sound waves, billow clouds (gravity waves), inertial oscillations, etc., but these are unimportant.*"

In his 1955 paper, [7], Charney discusses the characteristics of atmospheric motion by making the following assumption: he assumes that the

atmosphere is statically stable, by this he is assuming that the horizontal scale, L_H, is larger than the vertical, L_Z. He takes L_Z to be of the order of one atmospheric height, 10km, and the horizontal scale to be 100km. The effect of this is that the atmospheric motions are in *quasi-hydrostatic balance* and are of planetary scale, [34].

A consequence of the hydrostatic assumption is that there are no sound waves and the equations that govern such an atmosphere are the primitive equations, which we introduce in Section 2.3.

In [14], Daley defines two types of time scales that are observed in this type of atmosphere. These are given by

$$\tau_1 = \frac{1}{f}, \qquad \tau_2 = \frac{L_H}{V_H}, \tag{2.1}$$

where f is the Coriolis parameter and V_H is a characteristic horizontal velocity. These two time scales are referred to as the 'inertial' and 'advective' time scales respectively. The Rossby number associated with these scales is given by the ratio

$$R_0 = \frac{\tau_1}{\tau_2} = \frac{V_H}{L_H f}. \tag{2.2}$$

In the atmosphere R_0 is usually small. This implies that the advective time scale is much larger that the inertial time scale. The time scale τ_1 is usually a few hours whereas τ_2 is considered to be longer than a day.

There are two kinds of atmospheric motions that can be identified as

is to employ a filtering system in the receiver. Translating, the first method implies that the unwanted harmonics shall be eliminated from the raw data by some type of harmonic analysis; the second that you transform the equations of motion and make the approximations in such a way that the bad harmonics are automatically eliminated."

Charney is saying that there are two methods in which to perform the

n

unbalanced initial conditions for the model and a large projection onto the inertia-gravity mode of the equations.

An important thing to note is the atmosphere cannot be initialised but can be in balance. Initialisation is a process and can result in a balanced set of initial conditions.

In the next section we look at a way of initialising the shallow water equations to prevent the formation of inertia-gravity waves that are supported in this model.

. Shallow ater Theory

In this section we give a brief description of the shallow water model and the equations associated with this model. We also introduce the PV for this model and show that is materially invariant. Finally we give a review of an initialisation performed by Hinkelmann and Phillips to the shallow water equations.

2.2.1 Shallow Water Model

The underlying assumptions, as described in [34], for the shallow water model are that the flow is a sheet of fluid with constant and uniform density with a free surface height, h, where the fluid is assumed to be inviscid and in

rotation. The flow is also assumed to be incompressible. A diagram of the model is in Figure 2.1.

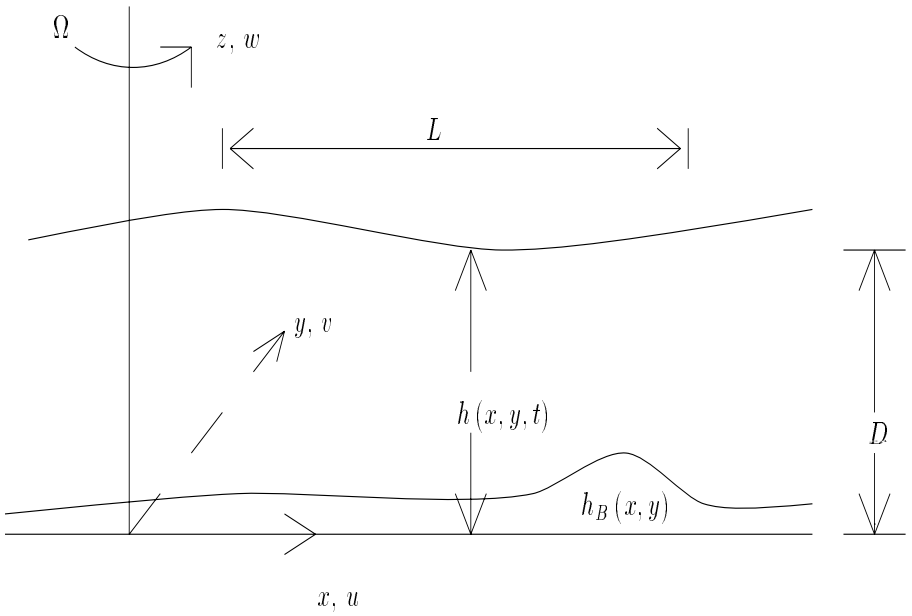

Figure 2.1: Diagram of the Shallow Water Model.

In Figure 2.1 the variable h is the height above a reference level $z = 0$ and is a function of the horizontal coordinates, x and y and time t, Ω is the rotation rate, u and v are the horizontal winds that are parallel to the horizontal coordinates, z is the vertical coordinate, w is the vertical wind which is parallel to the vertical axis, and h_B is the rigid bed of the fluid. Hence D is the depth, given by $h - h_B$, which does vary with time. For the scale analysis that allows us to consider these equations as a substitute for the atmosphere, we choose a sensi1hmTJ$^{-}\hat{}\hat{}$o

characterises shallow water theory is

$$\frac{D}{L} \ll 1. \tag{2.3}$$

Therefore we require the horizontal length scale to be considerably larger than the vertical scale.

2.2.2 Shallow Water Equations

The set of equations that govern this model is comprised of two momentum equations, one for each of the horizontal directions, and a continuity equation. These are given by

$$\begin{aligned} \frac{\partial u}{\partial t} + u\frac{\partial u}{\partial x} + v\frac{\partial u}{\partial y} - fv + g\frac{\partial h}{\partial x} &= 0, \\ \frac{\partial v}{\partial t} + u\frac{\partial v}{\partial x} + v\frac{\partial v}{\partial y} + fu + g\frac{\partial h}{\partial} & \end{aligned} \tag{2.4}$$

in their Eulerian form. The Lagrangian counterpart is given by

$$\frac{D\mathbf{u}}{Dt} + f\mathbf{k} \times \mathbf{u} = -g\nabla h, \tag{2.7}$$

$$\frac{Dh}{Dt} = -h\nabla \cdot \mathbf{u}, \tag{2.8}$$

where

$$\frac{D}{Dt} = \frac{\partial}{\partial t} + \mathbf{u} \cdot \nabla,$$

$\mathbf{k}$ is the z direction unit vector and $\nabla \cdot \mathbf{u}$ is the horizon

where δ represents the horizontal divergence. Rearranging (2.8) we obtain

$$\delta = -\frac{1}{h}\frac{Dh}{Dt}. \tag{2.11}$$

Substituting (2.11) into (2.10) gives

$$\frac{D}{Dt}(\xi + f) - \frac{(\xi + f)}{h}\frac{Dh}{Dt} = 0. \tag{2.12}$$

This can be written in the form

$$\frac{D}{Dt}\left(\frac{\xi + f}{h}\right. \quad = 0. \tag{2.13}$$

This last equation gives the information that the potential vorticity,

$$Q \equiv \frac{f + \xi}{h} = \frac{f + \frac{\partial v}{\partial x} - \frac{\partial u}{\partial y}}{h}, \tag{2.14}$$

is conserved following the motion of the vertical fluid columns. We will use the shallow water equations' potential vorticity in many of the following chapters but we now review an initialisation to the shallow water equations ,–towhic–tolumns.

a base state geopotential, $\bar{\Phi} = g\bar{h}$, which is only a function of y, where U is related to $\bar{\Phi}$ geostrophically through

$$U = -\frac{1}{f_0}\frac{\partial \bar{\Phi}}{\partial y}.$$

It is also assumed that the perturbations with respect to the velocity and the geopotential are only functions of x. When these assumptions are applied to equations (2.4) - (2.6) then the result is a much simpler set of equations.

Next stage in this process is to introduce the Helmholtz theorem that allows the wind field, $\mathbf{u}$, to be written in terms of derivatives of a stream function, ψ, and velocity potential, χ. This is given by

$$\mathbf{u} = \mathbf{k} \times \nabla\psi + \nabla\chi,$$

which in component form is

$$u = -\frac{\partial \psi}{\partial y} + \frac{\partial \chi}{\partial x}, \qquad v = \frac{\partial \psi}{\partial x} + \frac{\partial \chi}{\partial y}. \tag{2.15}$$

This can be used to write equations (2.4) - (2.6) in terms of ψ, χ and Φ. Next a wave solution is assumed for each of the three variables of the form

$$\begin{vmatrix} \psi(x,t) \\ \chi(x,t) \\ \Phi(x,t) \end{vmatrix} = \begin{vmatrix} \hat{\psi}_0(t) \\ \hat{\chi}_o(t) \\ \hat{\Phi}_0(t) \end{vmatrix} \exp\left[\frac{imx}{a} - \frac{iUmt}{a}\right], \tag{2.16}$$

where m is the x wave number, a is the radius of the Earth and the subscript denotes the variable at the initial time. These are then substituted into the

reduced equations and a Laplace transform is then applied to each of the three variables. The transfer function for

to zero. This removes the term $\frac{i\sigma_2\hat{\psi}_0}{\sigma_1^2}$ from (2.17) and in that case for there to be no inertia-gravity waves we must have the coefficients of the sine and cosine terms initially zero. This then gives the conditions

$$\hat{\chi}_0 = 0 \qquad \text{and} \qquad f_0\hat{\psi}_0 - \hat{\Phi}_0 = 0. \tag{2.19}$$

This condition is seen as a zeroth order initialisation state as it is saying that the initial state should be in geostrophic balance and that there should be a zero initial velocity potential.

If we now allow all the terms to stay in the reduced equations then this gives

$$\hat{\chi}_0 + \frac{i\sigma_2\hat{\psi}_0}{\sigma_1^2} = 0 \qquad \text{and} \qquad f_0\hat{\psi}_0 - \hat{\Phi}_0 = 0. \tag{2.20}$$

This is seen as a first order set of conditions, as w

move these from the more sophisticated models in 3-D, namely the primitive equations, (PE) and we do this in the next section.

.3 Primitive Equation Model

In the last section we summarised a technique to derive an initialisation to the 2-D non-linear shallow water equations to remove the inertia-gravity waves from the numerical model.

In this section we introduce the 3-D primitive equations and summarise a technique that initialises the PE such that the gravity waves are removed but also briefly look at the limitations of the method.

2.3.1 Primitive Equations

The primitive equations comprise of the equations of motion, (2.21), hydrostatic equation, (2.22), conservation of mass, (2.23), and the thermodynamic equation, (2.24). These are

$$\frac{\partial \mathbf{u}}{\partial t} + \mathbf{u}\cdot\nabla\mathbf{u} + \omega\frac{\partial \mathbf{u}}{\partial P} + f\mathbf{k}\times\mathbf{u} + \nabla\Phi = \mathbf{F}, \tag{2.21}$$

$$\frac{\partial \Phi}{\partial P} + \frac{RT}{P} = 0, \tag{2.22}$$

$$\nabla\cdot\mathbf{u} + \frac{\partial \omega}{\partial P} = 0, \tag{2.23}$$

$$\left(\frac{\partial}{\partial t} + \mathbf{u}\cdot\nabla \quad \frac{\partial \Phi}{\partial P} + \omega\Gamma = -\frac{RQ}{C_p P}, \right. \tag{2.24}$$

where P is the pressure and is used as the vertical coordinate system, $\omega \equiv \mathrm{d}P/\mathrm{d}t$ is the vertical velocity, R is the gas constant, C_P is the specific heat at constant pressure, T is the temperature and Φ is the geopotential, $\mathbf{F}$, is the frictional force per unit mass, Q here is the time rate of heating per unit mass, Γ is the static stability, ∇ is the gradient operator as defined in Appendix A and $\mathbf{u} = (u, v)^T$ is the horizontal wind field.

Firstly we nondimensionalise (2.21)-(2.24) using the following scales

- L_H is the horizontal scale (m)
- L_Z is the vertical scale (m)
- Π is the vertical pressure scale (mb)
- V_H is the horizontal winds speed (ms^{-1})
- N_0 is the Brunt-Väisälä frequency (s^{-1})
- $\frac{L_H}{V_H}$ is the advective time scale (s)
- g is the gravitational constant (ms^{-2})

The variables are nondimensionalised as follows

$$\begin{aligned} \mathbf{u}^* = V_H^{-1}\mathbf{u}, \qquad \nabla^* &= L_H\nabla, \qquad t^* = V_H L_H^{-1} t, \\ (x^*, y^*) = L_H^{-1}(x, y), \qquad P^* &= \Pi^{-1}P, \qquad \omega^* = L_H\Pi^{-1}V_H^{-1}\omega. \end{aligned} \tag{2.25}$$

The Coriolis parameter is approximated through a beta-plane as defined in Pedlosky, [34], given by

$$f^* = \frac{f}{2\Omega} = \left(f_0^* + \frac{L_H}{a} \beta^* y^* \right), \tag{2.26}$$

where $f_0^* = \sin\theta_0$ and $\beta^* = \cos\theta_0$

the mid-latitudes. The result is that the leading terms, in magnitude, are the Coriolis term and the geopotential gradients,

$$-fv \approx -\frac{\partial \Phi}{\partial x}, \qquad fu \approx -\frac{\partial \Phi}{\partial y}. \tag{2.32}$$

The two conditions in (2.32) are seen as first order approximations to the flow and is only valid for small Rossby numbers as explained in [17]. Therefore a flow is said to be *quasi-geostrophic* if the motion is nearly geostrophic.

To apply this approximation to (2.27) - (2.29) we require the parameters R_0, L_R and $\frac{L_H}{a} \ll 1$. If we consider

$$L_H = 10^6\text{m}, \quad L_Z = 10^4\text{m}, \quad V_H = 10\text{ms}^{-1}, \quad g = 10\text{ms}^{-2},$$

$$\Omega = 10^{-4}\text{s}^{-1}, \quad a = 10^7\text{m}, \quad N_0 = 10^{-2}\text{s}^{-1}, \quad L_R = 10^6\text{m},$$

to be typical values for the mid-latitudes, [14], then we see that the three parameters R_0, L_R and $\frac{L_H}{a}$ are around 0.1. We now introduce a small parameter, ε, that is the same magnitude as the Rossby number. This makes the three dimensionless numbers $O(\epsilon)$. We will use this information to initialise the model.

2.3.2 Quasi-Geostrophic Initialisation

Two possible methods to derive the quasi-geostrophic equations are; firstly expand the dependent variables u, v and Φ in an asymptotic series in terms

To derive a higher order set of conditions, we require the second time derivatives of u, v and Φ to be order one functions in ϵ. After many manipulations, for more details see [14], the final outcome is a version of the ***non-linear balance equation***, given by

$$\nabla^2\Phi - f\xi = -\varepsilon\left(\beta u_\psi + \nabla\cdot(\mathbf{u}_\psi\cdot\nabla\mathbf{u}_\psi)\right), \tag{2.38}$$

where u_ψ is the u component of $\mathbf{u}_\psi$.

The important feature of this equation is that it relates the stream function to the geopotential, through a Monge-Ampère type equation, to prevent motions of the same size as the inertia-gravity waves forming in the model. Therefore the initial data that satisfy (2.38) is balanced and integrating a primitive equations model with this data will not excite gravity waves.

We now consider briefly the limitations of the quasi-geostrophic initialisations to both the shallow w

This meant

$$R_0 = \frac{V_H}{2\Omega L_H}, \qquad \frac{L_H}{a}, \qquad \frac{R_0 L_H^2}{L_R^2},$$

were order ε. The main problem occurs when we start to enter the lower latitudes and the Rossby number is growing and as such the rotational flow associated with geostrophic flows is not correctly modelling the flow here. This restrains this type of initialisation to the mid-latitudes for best results.

.4 Summary

In this chapter was we have introduced the motivation and techniques for the removal of inertia-gravity waves from either a shallow water or primitive equations model.

There were two different techniques used to derive the initialisation. The first uses a Laplace transform and the other a bounded derivative method.

In the next chapter we consider a different approach to this problem by considering Hamiltonian dynamics and derive a different non-linear partial differential equation that also prevents these fast motions.

hapter 3

Balance Via Hamiltonian Dynamics

In the previous chapter we reviewed two initialisation techniques: one for the shallow water equations and the other for the primitive equations. For the primitive equations the process resulted in a non-linear balance equation, (2.38), where the stream function was related to the geopotential through a Monge-Ampère equation.

In this chapter we review other mathematical techniques to derive a balance equation. We start by introducing the basics of Hamiltonian dynamics, which will be used to derive a different balance equation. We then show how the shallow water equations can be derived in Hamiltonian dynamics through a variational principle. This is important as from this different balance equa-

There are two different ways of describing the continuum motion. The first is the Eulerian where the independent variables are the space coordinates, $\boldsymbol{x} = (x, y)$, and the time, t. The dependent variables are the height field, $h(x, y, t)$, and the velocities, $\mathbf{u}(x, y, t)$.

In the Lagrangian description, the independent variables are a set of

where F is a function of (x, y, t) or (a, b, τ). This leads to

$$\frac{\partial F}{\partial \tau} = \frac{\partial F}{\partial t} + u\frac{\partial F}{\partial x} + v\frac{\partial F}{\partial y} = \frac{\partial F}{\partial t} + \mathbf{u} \cdot \nabla F. \tag{3.3}$$

which is the form used in Section 2.2.1. A detailed derivation is given in [42].

With the basic description of fluid motions described here in terms of Lagrangian and Eulerian framework we now show how these are used in derivation of motions using Hamilton's principle.

3.1.1 Hamilton's Principle

Hamilton's principle states that the *action*

the $A \equiv \int_{t_1}^{t_2} L$L is La–LTˆˆTD–rangiaLTj¯TˆˆTˆˆT–andi–o–is–givTJˆˆ

Hi$\delta\beta\lambda$

hereLis theataθL

LparhtWiHBLe$\theta\delta$Tj∂TTTDtaL

Hamilton's principle states that the first variation of the action, δA, satisfies

$$\delta A \equiv \delta \int_{t_1}^{t_2} \left(\frac{1}{2} \sum_{i\ 1}^{N} m_i \frac{\mathrm{d}\mathbf{x}_i}{\mathrm{d}t} \cdot \frac{\mathrm{d}\mathbf{x}_i}{\mathrm{d}t} - V \quad \mathrm{d}t = 0, \tag{3.7}$$

for arbitrary, independent variations $\{\delta x_i(t), \delta y_i(t)\}$ that vanish at t_1 and t_2. Therefore we must have $\delta \mathbf{x}_i(t_1) = \delta \mathbf{x}_i(t_2) = 0$. From applying variational techniques we obtain

$$0 = \int_{t_1}^{t_2} \left(-m_i \frac{\mathrm{d}^2 \mathbf{x}_i}{\mathrm{d}t^2} - \frac{\mathrm{d}V}{\mathrm{d}\mathbf{x}_i} \quad \cdot \delta \mathbf{x}_i \mathrm{d}t. \right. \tag{3.8}$$

As a result of the arbitrariness of the variations the quantity inside the brackets must be zero. The result is Newton's second law.

For the second example we consider a barotropic fluid. The difference between the system of point masses and the fluid continuum is that the masses are distributed continuously in space in the continuum. Therefore, instead of a summation to represent the masses we have

$$\int\int\int \mathrm{d}m = \int\int\int \mathrm{d}a\mathrm{d}b\mathrm{d}c, \tag{3.9}$$

as derived in [42]. The kinetic energy is given by

$$T = \frac{1}{2} \int\int\int \mathrm{d}a\mathrm{d}b\mathrm{d}c \frac{\partial \mathbf{x}}{\partial \tau} \cdot \frac{\partial \mathbf{x}}{\partial \tau}. \tag{3.10}$$

For the potential energy we assume that this arises from external and interparticle forces that depend on the particle location $\mathbf{x}(a, b, c, \tau)$. The potential energy is

$$V = \int\int\int \mathrm{d}a\mathrm{d}b\mathrm{d}c \left(\quad (\alpha) + \phi(\mathbf{x}) \right), \tag{3.11}$$

where α is the specific volume and is given by

$$\alpha \equiv \frac{1}{\rho} = \frac{\partial(x,y,z)}{\partial(a,b,c)} = \begin{vmatrix} \frac{\partial x}{\partial a} & \frac{\partial x}{\partial b} & \frac{\partial x}{\partial c} \\ \frac{\partial y}{\partial a} & \frac{\partial y}{\partial b} & \frac{\partial y}{\partial c} \\ \frac{\partial z}{\partial a} & \frac{\partial z}{\partial b} & \frac{\partial z}{\partial c} \end{vmatrix} = \frac{\partial(\mathbf{x})}{\partial(\mathbf{a})},$$

ρ is the density and (α) is the specific internal energy and is a function of α, and $\phi(\mathbf{x}(\mathbf{a},t))$ is the external potential and is dependent on the fluid-particle locations.

This then gives the *action* for this system as

$$\int \mathrm{d}\tau\,(T-V) = \int \mathrm{d}\tau \iiint \mathrm{d}\mathbf{a} \left(\frac{1}{2}\frac{\partial \mathbf{x}}{\partial \tau} \cdot \frac{\partial \mathbf{x}}{\partial \tau} - \quad \left(\frac{\partial(\mathbf{x})}{\partial(\mathbf{a})} \quad - \phi(\mathbf{x}(\mathbf{a},\tau)) \quad , \right. \right. \tag{3.12}$$

which must be stationary with respect to the arbitrary variations $\delta\mathbf{x}(a,b,c,\tau)$, in the location of the fluid particles. A full derivation of the resulting equations can be found in [42].

We now extend these ideas to the shallow water equations, where in the next section we will define the Lagrangian for the shallow water equations as shown in [39] and derive the shallow water equations from this.

3. Hamiltonian Form for the Shallow ater Equations

In Salmon's 1983 and 1985 papers, [38] and [39], he shows that Hamilton's principle for a mechanical system with N degrees of freedom can be written in the form

$$\delta \int \mathrm{d}\tau \left(\sum_i p_i \frac{\partial q_i}{}$$

We shall return to the shallow water Lagrangian in Section 3.4 but we first describe an approximation made to (3.19) and (3.20). This approximation results in the *semi-geostrophic equations*. We look at this approximation in the next section and review certain properties that arise from this and extended these in Section 3.5.

3.3 Semi-Geostrophic Theory

In this section we will look at how the semi-geostrophic equations are derived from (3.19) and (3.20). We also look at the PV that is associated with these equations. We then give a review of the geostrophic coordinates that were devised b

winds, (2.32). This then leads to the equations

$$\dot{u}_g + g\frac{\partial h}{\partial x} - \dot{y}f = 0, \qquad \dot{v}_g + g\frac{\partial h}{\partial y} + \dot{x}f = 0. \tag{3.24}$$

These are referred to as the semi-geostrophic equations when they are combined with the continuity equation, (2.6).

This system has the Hamiltonian

$$\mathrm{H} = V + \int_{\mathcal{D}} \frac{1}{2}|\mathbf{u}_g|^2 \mathrm{d}m, \tag{3.25}$$

where $\mathcal{D}$ is the domain of interest and $\mathrm{d}m$ is the mass element, and

$$V = \int_{\mathcal{D}} \frac{1}{2} gh \mathrm{d}m, \tag{3.26}$$

is the potential energy of the mass configuration. There is a conserved quantity like potential vorticit

where ϕ is defined by

$$\phi(x, y, t) = \frac{g}{f^2} h(x, y, t). \tag{3.29}$$

This choice of ϕ enables us to write the definition of geostrophic winds, (2.32), as

$$u_g = -f\frac{\partial \phi}{\partial y}, \qquad v_g = f\frac{\partial \phi}{\partial x}. \tag{3.30}$$

This transformation, $\boldsymbol{x} \mapsto \boldsymbol{X}$

This then enables us to write the material derivative of the geostrophic coordinates in terms of Φ as

$$\dot{X} = -f\frac{\partial \Phi}{\partial Y}, \qquad \dot{Y} = f\frac{\partial \Phi}{\partial X}.$$

geostrophic winds are substituted in, gives

$$Q_{sg} = \frac{1}{h}\left(f + \left(\frac{\partial^2\phi}{\partial x^2} + \frac{\partial^2\phi}{\partial y^2}\right. \right. \left. - \frac{1}{2f}\left(\frac{\partial^2\phi}{\partial x^2}\frac{\partial^2\phi}{\partial y^2} - \left(\frac{\partial^2\phi}{\partial x \partial y}\right.^2\right)\right). \tag{3.38}$$

This partial differential equation is referred to as a ***Monge-Ampère Equation***. There is a condition on the equation to ensure solvablility but first we give the general form of the Monge-Ampère equation as expressed in [31] and then give this condition.

The general form of the Monge-Ampère equation is

$$A + Br + 2Cs + Dt + \left(rt - s^2\right) = 0, \tag{3.39}$$

where for (x, y) space we can define p, q, r, s and t to be

$$p = \frac{\partial\phi}{\partial x}, \;\; q = \frac{\partial\phi}{\partial y}, \;\; r = \frac{\partial^2\phi}{\partial x^2}, \;\; s = \frac{\partial^2\phi}{\partial x \partial y}, \;\; t = \frac{\partial^2\phi}{\partial y^2}, \tag{3.40}$$

where A, B, C, D and are given functions of (x, y, ϕ, p, q). It must be noted that p and q are the general notation used in [31]. The solvability condition for non-linear second order partial differential equations is

$$BD - C^2 - A \quad > 0, \tag{3.41}$$

and is referred to autfi–nellipticiedTJ¯T^^Tf¯y^^TDcns[erto

tions if

$$BD - C^2 - A \quad > 0,$$

and the coefficients in (3.39) are all continuous in the domain.

Returning to (3.38) then, after we have multiplied throughout by $\frac{h}{f}$, we have the following coefficients $B = D = 1, C = 0, \quad = 1$ and $A = 1 - \frac{Q_{sg}h}{f}$. Then evaluating (3.41) gives us the condition $Q_{sg} > 0$ which was assumed in Section 3.3.2. In [31] they derive the condition for the transformed variable and arrive at the same condition for the PV.

In Section 3.5 we derive another Monge-Ampère equation whose solutions gives a balanced height field. Before this we return to the Hamiltonian dynamics to explain a series of approximations to the shallow water Lagrangian that were performed by Salmon, [38], [39], which results in an initialisation through Hamiltonian dynamics.

3.4 Salmon's L_0 and L_1 Dynamics

In Section 3.2 we introduced the Lagrangian for the shallow water equations, (3.16), as derived in [38]. We now summarise two approximations that Salmon makes to this functional which result in sets of initial conditions for the shallow water equations, and yet have a Hamiltonian structure associated

geophysical fluid dynamics. He suggests not dropping the wind field but to replace them with the geostrophic winds. He labels this approximation L_1.

3.4.2 L_1 Dynamics

We return to the full Lagrangian for the shallow water equations, where Salmon now uses the geostrophic winds, (u_g, v_g), which are dependent on the height field, as an approximation to the full wind fields. The resulting Lagrangian is labelled L_1 and is given by

$$L_1 = \int\int \mathrm{d}a\mathrm{d}b \left((u_g - R) \frac{\partial x}{\partial \tau} + (v_g + P) \frac{\partial y}{\partial \tau} - \frac{1}{2} \left(u_g^2 + v_g^2 + g \frac{\partial (a,b)}{\partial (x,y)} \right. \right. \quad . \tag{3.46}$$

L_1 is still dependent only on the particle locations as the geostrophic winds are determined by the mass distribution.

To apply Hamilton's principle to L_1, Salmon introduces variations to x, y, u_g, v_g, h, R and P. Substituting these quantities into (3.46) and ignoring terms of $O(\delta^2)$ gives

$$\int\int \mathrm{d}a\mathrm{d}b \, (u_g - R) \frac{\partial \delta x}{\partial \tau} + (v_g + P) \frac{\partial \delta y}{\partial \tau} - \dot{x}\delta R + \dot{y}\delta P + (\dot{\mathbf{x}} - \mathbf{u}_G) \cdot \delta \mathbf{u}_g - \frac{1}{2} g \delta h. \tag{3.47}$$

Salmon now introduces the ageostrophic velocity, which he defines to be

$$\mathbf{u}_{ag} \equiv \frac{\partial \mathbf{x}}{\partial \tau} - \mathbf{u}_g. \tag{3.48}$$

The next step is to integrate (3.47) and then substitute (3.48). This then results in

$$\int\int \left(-\dot{u}_g + f\dot{y}\right)\delta x + \left(-\dot{v}_g - f\dot{x}\right)\delta y + \mathbf{u}_{ag}\cdot\delta\mathbf{u}_g - \frac{1}{2}g\delta h. \tag{3.49}$$

The final stage of the derivation to the equations is shown in Appendices A and B in [39]. The resulting equations in an Eulerian framework are the momentum equations

$$h\left(\frac{\partial}{\partial t}\mathbf{u}_g + \mathbf{u}_g\cdot\nabla\mathbf{u}_g + \mathbf{u}_{ag}\cdot\nabla\mathbf{u}_g + \mathbf{u}_{ag}\cdot\nabla\mathbf{u}_g \quad + f\mathbf{k}\times h\left(\mathbf{u}_g + \mathbf{u}_{ag}\right) + g\nabla\left(\frac{1}{2}h^2\right)\right.$$
$$= -g\nabla\left(h^2\mathbf{k}\cdot\nabla\times\left(\frac{\mathbf{u}_{ag}}{f}\right.\right. \quad - g\nabla\left(\frac{1}{2}h^2\right)\left(\mathbf{u}_{ag}\times\nabla\left(\frac{1}{f}\right.\right. \quad \cdot\mathbf{k}, \tag{3.50}$$

and a continuity equation

$$\frac{\partial h}{\partial t} + \nabla\cdot\left(\left(\mathbf{u}_g + \mathbf{u}_{ag}\right)h\right) = 0. \tag{3.51}$$

To simplify equations (3.50) and (3.51) Salmon uses the information that every Hamiltonian system is precisely defined by the two geometrical objects: the Poisson-bracket operator and the Hamiltonian itself, [39], [41]. We will not go into how Salmon manages to derive the results but there is a full explanation in [39].

Salmon notices that it is possible to define a set of canonical coordinates that enables the Poisson-bracket operator to take its simplest form. He then applies these coordinates to the shallow water Lagrangian and then applies the variations with respect to these coordinates. The result is the coordinates

derived by Hoskins, [21], and the resulting dynamical equations are the semi-geostrophic equations in 2-D for a constant f, which show that the potential vorticity for these equations, (3.27), is conserved.

One final remark from [39] is the description that Salmon has for the reduced dynamics. Salmon says that the approximations $L \approx L_0$ and $L \approx L_1$ can be viewed as projections of the fluid state vector in the infinite dimensional phase space spanned by $\{x, y, u, v\}$ onto the subspace spanned by $\{x, y\}$. For L_0 the projected coordinates $\{u, v\}$ are set to zero whereas for L_1 these are replaced by the geostrophic values, (u_g, v_g).

In [41] Salmon gives a mathematical interpretation for the approximations that he has applied. In the paper he shows that the semi-geostrophic approximation is a specific projection onto the phase space manifold corresponding to geostrophic balance. Associated with these is a set of canonical coordinates. He goes on to derive the expression for the balanced part of the phase space in terms of the approximation to the wind field, $\mathbf{u}$, and he shows that for the semi-geostrophic approximation the subspace in the phase space is given by

$$\mathbf{u}_s^c \equiv \mathbf{u}_g - \frac{1}{2f} \left(\mathbf{u}_g \cdot \nabla\right) \left(\mathbf{k} \times \mathbf{u}_g\right). \tag{3.52}$$

In [41], Salmon comments that it would be possible to make further approximations of higher order to the wind field that would also have a subspace

associated with them. McIntyre and Roulstone extend this theory from the

which is of the same form as in Section 2.2.2.

The constrained wind field $\mathbf{u}_s^c$ is the expression given for the subspace for the semi-geostrophic balance, (3.52). Equation (3.55) is the same as (3.27).

We next describe the work undertaken by McIntyre and Roulstone where they extend the ideas by Salmon.

3.5.2 Higher Order Balance

In [31], McIntyre and Roulstone note that the constrained wind field, $\mathbf{u}_s^c$, that Salmon derived for the slow manifold, (3.52), is both a field and a mass-configuration functional. They denote this by

$$\mathbf{u}^c \equiv \mathbf{u}^c\left(\mathbf{x}; h\left(\cdot\right)\right). \tag{3.56}$$

They make useful comments on how to view the constraint as a splitting of the parent velocity field, $\mathbf{u}^p$

McIntyre and Roulstone then derive an extension to the canonical coordinates that Salmon uses to derive the semi-geostrophic equations form. They are able to derive a set of set of canonical coordinates so that the PV can be written in the form

$$Q^c = \frac{f}{h}\frac{\partial(X,Y)}{\partial(x,y)}, \tag{3.58}$$

where the canonical coordinates are given by

$$\boldsymbol{X} = \mathbf{x} + \nabla\phi - i\gamma\mathbf{k}\times\nabla\psi, \tag{3.59}$$

where $i = \sqrt{-1}$ and $\gamma = \sqrt{(2\alpha+1)}$. They show that the α in (3.59) is related to the sub-spaces by

$$\mathbf{u}^c = \frac{1}{2}f\mathbf{k}\times\mathbf{x} + \mathbf{u}_g + \frac{\alpha}{f}\mathbf{u}_g\cdot\nabla\left(\mathbf{k}\times\mathbf{u}_g\right). \tag{3.60}$$

To obtain the form for the semi-geostrophic model, (3.52), we substitute $\alpha = -\frac{1}{2}$ -9yT--+1pJ^^Tf^^T^Tc--(3.59)Tj-e-^^TD--u-

the condition derived in Section 3.3.3. For the third situation we have $\alpha = 1$ and $\gamma = \sqrt{3}$ and as such the equation is elliptic if $\frac{\zeta^c}{f} < \frac{3}{2}$ which is satisfied provided that the sub-space actually approximates the slow moving manifold and this is so only when we have the Rossby number small.

The balanced wind field defined by (3.61) has the property that for constant f this is not divergence free. Therefore if we could use this to find a balanced height then the associated $\mathbf{u}^c$ with this would be a divergent rotational balanced wind.

This is possible by calculating the relative vorticity from $\mathbf{u}^c$ and we do that here

$$\begin{aligned}
\xi^c &= \mathbf{k}\cdot\nabla\times\mathbf{u}^c = \mathbf{k}\cdot\nabla\times\mathbf{u}_g + \frac{1}{f}\mathbf{k}\cdot\nabla\times(\mathbf{u}_g\cdot\nabla)(\mathbf{k}\times\mathbf{u}_g) \\
&= \frac{g}{f}\nabla^2 h + \frac{1}{f}\mathbf{k}\cdot\nabla\times\left(-\left(u_g\frac{\partial v_g}{\partial x} + v_g\frac{\partial v_g}{\partial y}\right.\right. \quad \mathbf{i} + \left(u_g\frac{\partial u_g}{\partial x} + v_g\frac{\partial u_g}{\partial y}\right. \quad \mathbf{j} \\
&= \frac{g}{f}\nabla^2 h + \frac{1}{f}\left(\frac{\partial}{\partial x}\left(u_g\frac{\partial u_g}{\partial x} + v_g\frac{\partial u_g}{\partial y}\right.\right. \quad \frac{\partial}{\partial y}\left(u_g\frac{\partial v_g}{\partial x} + v_g\frac{\partial v_g}{\partial y}\right. \\
&= \frac{g}{f}\left(\frac{\partial^2 h}{\partial x^2} + \frac{\partial^2 h}{\partial y^2}\right. \quad - \frac{2g^2}{f^3}\left(\frac{\partial^2 h}{\partial x^2}\frac{\partial^2 h}{\partial y^2} - \left(\frac{\partial^2 h}{\partial x\partial y}\right.\right.^2\Bigg), \qquad (3.64)
\end{aligned}$$

which has the following coefficients for the ellipticity condition: $A = \frac{f^3\xi^c}{2g^2}$, $B = D = -\frac{f^2}{2g^2}$, $C = 0$ and $\quad = 1$. This then gives a condition of $\frac{f}{2} > \xi^c$.

It is from this last Monge-Ampère equation and the equation arising from forming ξ^c when $\alpha = 0$ that the rest of the thesis is concerned with.

associated with these.

In [41], Salmon gives a mathematical structure to the approximations he mak

hapter 4

Balance Equations on the

(2.20), required again some form of geostrophic balance but now with a non-zero velocity potential. These are seen as differing in that the second conditions allow for an initial divergence.

In Section 2.3 we reviewed a method that nondimensionalised the primitive equations so that the time scale was that of the advective scale. To these equations a bounded derivative method was applied. Through bounding the first time derivatives to be $O(1)$ we arrived at (2.37), which is the geostrophic balance condition. By bounding the second derivatives we arrive at an equation that links the geopotential to the stream function, (2.38). This is referred to as a non-linear balance equation, [14], [54].

In Section 3.3 we in[illegible] o s t d i t – 3

using information about the structure of Hamiltonian dynamics, Salmon is able to define a subspace in the phase space of the shallow water equations where the semi-geostrophic motions lie, (3.52).

In Section 3.5 we reviewed [30] and [31] where McIntyre and Roulstone extend the subspace to a more generalised form as Salmon suggests in [41], to link a set of sub-spaces that represent the slow motions in the shallow water equations to a set of canonical coordinates, (3.59) with (3.60), and enables the PV to be written in the Jacobian form, (3.58).

One of these sub-spaces is given by

$$\mathbf{u}^c = \mathbf{u}_g + \frac{1}{f}\left(\mathbf{u}_g \cdot \nabla\right)\left(\mathbf{k} \times \mathbf{u}_g\right),$$

(3.61, which is the same as the Rossby number expansion for the wind fields correct to second order, [31], [47]. This is also defining a balanced wind.

In this chapter we develop the mathematics necessary to calculate a balanced height through the same approach that we described at the end of Section 3.5.2, but on the sphere. We also derive the spherical component form for the balanced wind and the spherical version of the Monge-Ampère equation given in Cartesian coordinates by (3.64).

We then modify this technique to be able to use this with an incremental data assimilation scheme. We achieve this by linearising the spherical definition of the balanced wind field and following the same procedure for

calculating ξ^c as in Section 3.5.2.

We also derive a linearised version of Q^c associated with (3.61) for the sphere. The result is a variable coefficient Poisson equation for the relative vorticity and a variable coefficient Helmholtz equation for the PV. The solution of these equations is a balanced height increment from which we can reconstruct the balanced wind field. If $\alpha = 1$ in the spherical version of (3.61) then the resulting wind field is divergent for constant f.

As we are concerned with the possibility of using this variable in a variational data assimilation scheme, we briefly describe the current control variable transforms employed in the Met. Office's incremental 3-D variational data assimilation scheme, (3D VAR), and then explain how the balanced height could be used as an alternative to the stream function and introduce two new unbalanced variables in the last section.

We begin with a brief derivation of the shallow water equations as this

4.1 Spherical S E and Balance

The aim of this section is to introduce the spherical shallow water equations and then to derive the spherical version of the non-linear balance equation. This is the equivalent to the Cartesian version that can be found following the derivation in [34]. To arrive at the spherical version we follow the proof set out in [22].

4.1.1 Spherical Shallow Water Equations

We recall the vectorial version of the Cartesian form of the shallow water equations in Section 2.2.2, (2.7) and (2.8). We start with (2.7),

$$\frac{D\mathbf{u}}{Dt} + f\mathbf{k} \times \mathbf{u} = -g\nabla h.$$

Writing in coq–kTj¯o¯Q¯BT¯Tˆ–of–n–[–22–].¯u–.non-linear

continuity equation, (2.6), as

$$\frac{\partial h}{\partial t} + \frac{u}{a\cos\theta}\frac{\partial h}{\partial \lambda} + \frac{v}{a}\frac{\partial h}{\partial \theta} + \frac{h}{a\cos\theta}\left(\frac{\partial u}{\partial \lambda} + \frac{\partial (\cos\theta v)}{\partial \theta}\right. = 0. \qquad (4.3)$$

Therefore, equations (4.1), (4.2) and (4.3) are the spherical version of the shallow water equations.

4.1.2 Spherical Non-Linear Balance Equation

In Section 2.3 we summarised an initialisation technique that resulted in a non-dimensional non-linear balance equation, (2.38). To derive the dimensional spherical version of (2.38) we consider the spherical version of the equations of motion for the 3-D primitive equations model, (2.21). We make the assumption of homogeneity and ignore the vertical wind, [54]. The remaining terms are similar to the spherical version of the shallow water equations, (4.1) and (4.2), but with geopotential gradients rather than height gradients.

We start by taking the divergence of the equations and ignoring the time derivative of the divergence. The reason for this is that the removal of this term 'filters' the inertia-gravity waves, [54]. The remaining terms are

$$\nabla \cdot ((\mathbf{u} \cdot \nabla)\,\mathbf{u}) + \nabla^2 \Phi + \nabla \cdot (f\mathbf{k} \times \mathbf{u}) = 0. \qquad (4.4)$$

Expanding the term $\nabla \cdot (\mathbf{u} \cdot \nabla)\,\mathbf{u}$ using the spherical definitions in Ap-

pendix A gives

$$\frac{1}{a^2\cos^2\theta}\left(\left(\frac{\partial u}{\partial\lambda}\right)^2+u\frac{\partial^2 u}{\partial\lambda^2}\right)+\frac{1}{a^2\cos\phi}\left(2\frac{\partial v}{\partial\lambda}\frac{\partial u}{\partial\theta}+u\frac{\partial^2 v}{\partial\theta\partial\lambda}+v\frac{\partial^2 u}{\partial\lambda\partial\theta}\right.$$
$$-\frac{\tan\phi}{a^2\cos\theta}\left(v\frac{\partial u}{\partial\lambda}+2u\frac{\partial v}{\partial\lambda}\right)-\frac{\tan\theta}{a^2}v\frac{\partial v}{\partial\theta}+\left(\frac{1}{a^2\cos\theta}-\frac{\tan^2\theta}{a^2}\right)u^2$$
$$+\frac{1}{a^2}\left(\left(\frac{\partial v}{\partial\theta}\right)^2+v\frac{\partial^2 v}{\partial\theta^2}+\frac{2\tan\theta}{a^2}u\frac{\partial u}{\partial\theta}\right)=\nabla\cdot(\mathbf{u}\cdot\nabla)\,\mathbf{u}. \quad (4.5)$$

In the next step we use the trigonometric identity $\sec^2\theta=\tan^2\theta+1$. We now use the Helmholtz theorem for the wind field,

$$\mathbf{u}=\mathbf{k}\times\nabla\psi+\nabla\chi,$$

which in spherical coordinates, where we are only considering the balanced component,

$$u=-\frac{1}{a}\frac{\partial\psi}{\partial\theta},\qquad v=\frac{1}{a\cos\theta}\frac{\partial\psi}{\partial\lambda}. \quad (4.6)$$

Substituting (4.6) into (4.5) gives

$$\nabla\cdot(\mathbf{u}\cdot\nabla)\,\mathbf{u}=\frac{1}{a^4\cos^2\theta}\left(2\left(\frac{\partial^2\psi}{\partial\theta\partial\lambda}\right)^2-2\frac{\partial^2\psi}{\partial\lambda^2}\frac{\partial^2\psi}{\partial\theta^2}+4\tan\theta\frac{\partial\psi}{\partial\lambda}\frac{\partial^2\psi}{\partial\theta\partial\lambda}\right.$$
$$\left.+\left(2\tan^2\theta+1\right)\left(\frac{\partial\psi}{\partial\theta}\right)^2\right)+\frac{1}{a^4}\left(\frac{\partial\psi}{\partial\theta}\right)^2+\frac{2\tan\theta}{a^4}\frac{\partial\psi}{\partial\theta}\frac{\partial^2\psi}{\partial\theta^2}. \quad (4.7)$$

In (4.7) the third order terms have cancelled. We now consider the divergence

Substituting (4.6) for the wind field and differentiating the Coriolis parameter gives

$$\nabla \cdot (f\mathbf{k} \times \mathbf{u}) - \frac{1}{}$$

4. New Non-Linear Balance Equation

In this section we derive an alternative balance equation to (4.10) to find a balanced height. We derive the equation from the general form of the balanced wind field, (3.60) with the first term ignored, and then find the form of the equation for $\alpha = 0$ and 1.

We begin by recalling the general form of the balanced wind field, (3.60),

$$\mathbf{u}^c = \mathbf{u}_g + \frac{\alpha}{f}\mathbf{u}_g \cdot \nabla \left(\mathbf{k} \times \mathbf{u}_g\right), \tag{4.11}$$

where we have removed the first term to calculate the relative vorticity. To find its spherical form we use the spherical expression given in Appendix A. Therefore, in component form this is

$$u^c = u_g - \frac{\alpha}{f}\left(\frac{u_g}{a\cos\theta}\partial v_g\right.$$

We now introduce the height version of the geostrophic winds in spherical coordinates. These are

$$u_g \equiv -\frac{g}{f}\frac{\partial h}{\partial \theta}, \qquad v_g \equiv \frac{g}{fa\cos\theta}\frac{\partial h}{\partial \lambda}. \tag{4.16}$$

To derive the Monge-Ampère equation we substitute (4.16) into (4.15). The result is

$$\begin{aligned}\xi^c = \frac{g}{fa^2}\Bigg(&\frac{1}{\cos^2\theta}\frac{\partial^2 h}{\partial\lambda^2} + \frac{\partial^2 h}{\partial\theta^2} - \tan\theta\frac{\partial h}{\partial\theta} \quad + \frac{2g^2\alpha}{f^3a^4\cos^2\theta}\Bigg(\Bigg(\frac{\partial^2 h}{\partial\theta\partial\lambda}\quad^2\\ &-\frac{\partial^2 h}{\partial\lambda^2}\frac{\partial^2 h}{\partial\theta^2} + 2\tan\theta\frac{\partial h}{\partial\lambda}\frac{\partial^2 h}{\partial\theta\partial\lambda} + 2\tan^2\theta\left(\frac{\partial h}{\partial\lambda}\quad^2 + \sin\theta\cos\theta\frac{\partial h}{\partial\theta}\frac{\partial^2 h}{\partial\theta^2}\right.\right.\\ &\left.\left.+\frac{1}{2}\left(\left(\frac{\partial h}{\partial\lambda}\quad^2 + \cos^2\theta\left(\frac{\partial h}{\partial\theta}\quad^2\right)\right)\right).\end{aligned} \tag{4.17}$$

In the expression above all the third order terms have cancelled out. To obtain this expression we have assumed a constant f. This is often referred to the f plane approximation, [54], which is often used as a first stage of testing of new model variables.

If we consider the geostrophic sub-space, $\alpha = 0$, then (4.17) simplifies to

$$\xi^c = \frac{g}{fa^2}\left(\frac{1}{\cos^2\theta}\frac{\partial^2 h}{\partial\lambda^2} + \frac{\partial^2 h}{\partial\theta^2} - \tan\theta\frac{\partial h}{\partial\theta}\right), \tag{4.18}$$

which is a spherical Poisson equation. If we take $\alpha = 1$ then the result is

$$\begin{aligned}\xi^c = \frac{g}{fa^2}\Bigg(&\frac{1}{\cos^2\theta}\frac{\partial^2 h}{\partial\lambda^2} + \frac{\partial^2 h}{\partial\theta^2} - \tan\theta\frac{\partial h}{\partial\theta} \quad + \frac{2g^2}{f^3a^4\cos^2\theta}\Bigg(\Bigg(\frac{\partial^2 h}{\partial\theta\partial\lambda}\quad^2\\ &-\frac{\partial^2 h}{\partial\lambda^2}\frac{\partial^2 h}{\partial\theta^2} + 2\tan\theta\frac{\partial h}{\partial\lambda}\frac{\partial^2 h}{\partial\theta\partial\lambda} + 2\tan^2\theta\left(\frac{\partial h}{\partial\lambda}\quad^2 + \sin\theta\cos\theta\frac{\partial h}{\partial\theta}\frac{\partial^2 h}{\partial\theta^2}\right.\right.\\ &\left.\left.+\frac{1}{2}\left(\left(\frac{\partial h}{\partial\lambda}\quad^2 + \cos^2\theta\left(\frac{\partial h}{\partial\theta}\quad^2\right)\right)\right).\end{aligned}$$

We now consider an extension to ξ^c to form the constrained potential vorticity, Q^c. We start from the definition

$$Q^c \equiv \frac{f + \xi^c}{h} \equiv \frac{\zeta^c}{h}, \tag{4.19}$$

where we would substitute the righ

However, we do not use (4.19) to define the PV but a linearised form that we derive in Section 4.3.3.

4.3.1 Linearised Balanced Wind Field

The non-linear aspect of the balanced wind field, (3.61), arises from the term $\mathbf{u}_g \cdot \nabla (\mathbf{k} \times \mathbf{u}_g)$. To linearise this we introduce a base state for the height and consider increments to this. We start by expressing the height field, h, as $h = \bar{h} + h'$, where $\bar{h}$ is a base state height and h' is an increment. The geostrophic wind then becomes

$$\mathbf{u}_g = \bar{\mathbf{u}}_g + \mathbf{u}'_g, \tag{4.21}$$

where

u

$$v^{c\prime} \equiv v'_g + \frac{\alpha}{f}\left(\frac{u'_g}{a\cos\theta}\frac{\partial \bar{u}_g}{\partial\lambda} + \frac{\bar{u}_g}{a\cos\theta}\frac{\partial u'_g}{\partial\lambda} + \frac{v'_g}{a}\frac{\partial \bar{u}_g}{\partial\theta} + \frac{\bar{v}_g}{a}\frac{\partial u'_g}{\partial\theta}\right.$$
$$\left. - \frac{\tan\theta}{a}\left(u'_g\bar{v}_\chi\right.\right.$$

where, for convenience, we use Γ_1 to represent the first derivative of f^{-1} and Γ_2, the second derivative with respect to θ. Therefore these are

$$\Gamma_1 = \frac{\partial}{\partial\theta}\left(\frac{1}{f}\right. \quad , \qquad \Gamma_2 = \frac{\partial^2}{\partial\theta^2}\left(\frac{1}{f}\right. \quad . \tag{4.29}$$

The next term in (4.27) is $\mathbf{k}\cdot\nabla\times\left(\bar{\mathbf{u}}_g\cdot\nabla\left(\mathbf{k}\times\mathbf{u}'_g\right)\right)$. Evaluating $\bar{\mathbf{u}}_g\cdot\nabla\left(\mathbf{k}\times\mathbf{u}'_g\right)$ gives

$$\bar{\mathbf{u}}_g\cdot\nabla\left(\mathbf{k}\times\mathbf{u}'_g\right) = \frac{\bar{u}_g}{a\cos\theta}\frac{\partial}{\partial\lambda}\left(-\mathbf{i}v'_g+\mathbf{j}u'_g\right)+\frac{\bar{v}_g}{a}\frac{\partial}{\partial\theta}\left(-\mathbf{i}v'_g+\mathbf{j}u'_g\right).$$

Taking the differential operators through gives

$$\begin{aligned}\bar{\mathbf{u}}_g\cdot\nabla\left(\mathbf{k}\times\mathbf{u}'_g\right) &= -\left(\frac{\bar{u}_g}{a\cos\theta}\frac{\partial v'_g}{\partial\lambda}+\frac{\bar{u}_g}{a}\frac{\partial v'_g}{\partial\theta}+\frac{\tan\theta}{a}\bar{u}_g u'_g\right. \quad \mathbf{i}\\ &\quad +\left(\frac{\bar{u}_g}{a\cos\theta}\frac{\partial u'_g}{\partial\lambda}+\frac{\bar{v}_g}{a}\frac{\partial u'_g}{\partial\theta}-\right. \quad +\mathrm{Tf}^{-}\hat{}\hat{}\mathrm{TD}^{-}\text{–}\mathrm{gTj}^{-}\mathrm{fi}.\end{aligned}$$

Substituting (4.31) and (4.32) into the right hand side of (4.33) gives

$$\mathbf{k}\cdot\nabla\times\left(\mathbf{u}_g'\cdot\nabla\left(\mathbf{k}\times\bar{\mathbf{u}}_g\right)\right)=\frac{1}{a\cos\theta}\left(\overbrace{\frac{\partial}{\partial\lambda}\left(\frac{\bar{u}_g}{a\cos\theta}\frac{\partial u_g'}{\partial\lambda}\right.}^{T_1}+\overbrace{\frac{\partial}{\partial\lambda}\left(\frac{\bar{v}_g}{a}\frac{\partial u_g'}{\partial\theta}\right.}^{T_2}\right.$$

$$\left.-\underbrace{\frac{\partial}{\partial\lambda}\left(\frac{\tan\theta}{a}\bar{u}_g v_g'\right.}_{T_3}+\underbrace{\frac{\partial}{\partial\theta}\left(\frac{\bar{u}_g}{a}\frac{\partial v_g'}{\partial\lambda}\right.}_{T_4}+\underbrace{\frac{\partial}{\partial\theta}\left(\frac{\cos\theta}{a}\bar{v}_g\frac{\partial v_g'}{\partial\theta}\right.}_{T_5}+\underbrace{\frac{\partial}{\partial\theta}\left(\frac{\sin\theta}{a}\bar{u}_g u_g'\right.}_{T_6}\right). \tag{4.34}$$

For the remainder of the derivation of $\mathbf{k}\cdot\left(\nabla\times\left(\bar{\mathbf{u}}_g\cdot\nabla\left(\mathbf{k}\times\mathbf{u}_g'\right)\right)\right)$ we substitute (4.22) for the incremental height and use the variables, h, u_g, v_g, to represent $h', \bar{u}_g, \bar{v}_g$ respectively.

The first term, T_1, in (4.34) is

$$T_1=\frac{\partial}{\partial\lambda}\left(\frac{u_g}{a\cos\theta}\frac{\partial}{\partial\lambda}\left(-\frac{g}{af}\frac{\partial h}{\partial\theta}\right.\right.\quad=-\frac{g}{a^2 f\cos\theta}\left(\cos\right.$$

The fourth term, T_4, involves the derivative of $\sec\theta$ which is $\tan\theta\sec\theta$. Using this information and Γ_1 from (4.29) makes

$$T_4 = \frac{\partial}{\partial\theta}\left(\frac{gu_g}{a^2 f\cos\theta}\frac{\partial^2 h}{\partial\lambda^2}\right. = \frac{g}{a^2 f\cos\theta}\frac{\partial u_g}{\partial\theta}\frac{\partial^2 h}{\partial\lambda^2} + \frac{u_g}{a^2}\frac{\partial}{\partial\theta}\left(\frac{g}{f\cos\theta}\frac{\partial^2 h}{\partial\lambda^2}\right. =$$
$$\frac{g}{a^2 f\cos\theta}\left(\frac{\partial u_g}{\partial\theta}\frac{\partial^2 h}{\partial\lambda^2} + \tan\theta u_g\frac{\partial^2 h}{\partial\lambda^2} + u_g\frac{\partial^3 h}{\partial\lambda^2\partial\theta}\right. + \frac{\Gamma_1}{a^2\cos\theta}u_g\frac{\partial^2 h}{\partial\lambda^2}. \quad (4.38)$$

The fifth term, T_5, is broken down into three parts. The first, T_{5a}, is

$$T_{5a} = \frac{\cos\theta}{a}\frac{\partial v_g}{\partial\theta}\frac{\partial}{\partial\theta}\left(\frac{g}{af\cos\theta}\frac{\partial h}{\partial\lambda}\right. = \frac{g\tan\theta}{a^2 f}\frac{\partial v_g}{\partial\theta}\frac{\partial h}{\partial\lambda} + \frac{g}{a^2 f}\frac{\partial v_g}{\partial\theta}\frac{\partial^2 h}{\partial\lambda\partial\theta} + \frac{g\Gamma_1}{a^2 f}\frac{\partial v_g}{\partial\theta}\frac{\partial h}{\partial\lambda}. \quad (4.39)$$

The second part, T_{5b}, is

$$T_{5b} = -\frac{\sin\theta v_g}{a}\frac{\partial}{\partial\theta}\left(\frac{g}{af\cos\theta}\frac{\partial h}{\partial\lambda}\right. = -\frac{g\tan^2\theta}{a^2 f}v_g\frac{\partial h}{\partial\lambda} - \frac{g\tan\theta}{a^2 f}v_g\frac{\partial^2 h}{\partial\theta\partial\lambda}$$
$$-\frac{g\tan\theta\Gamma_1}{a^2}v_g\frac{\partial h}{\partial\lambda}. \quad (4.40)$$

The third part, T_{5c}, is the largest and most complicated. The first part of

We now derive $\mathbf{k} \cdot \left(\nabla \times \left(\mathbf{u}_g' \cdot \nabla \left(\mathbf{k} \times \bar{\mathbf{u}}_g \right) \right) \right)$ from (4.27). The result is

$$\mathbf{k} \cdot \left(\nabla \times \left(\mathbf{u}_g' \cdot \nabla \left(\mathbf{k} \times \bar{\mathbf{u}}_g \right) \right) \right) = \frac{1}{a \cos\theta} \left(\overbrace{\frac{\partial}{\partial \lambda} \left(\frac{u_g'}{a \cos\theta} \frac{\partial \bar{u}_g}{\partial \lambda} \right.}^{T_1} + \overbrace{\frac{\partial}{\partial \lambda} \left(\frac{v_g'}{a} \frac{\partial \bar{u}_g}{\partial \theta} \right.}^{T_2} \right.$$

$$\left. - \underbrace{\frac{\partial}{\partial \lambda} \left(\frac{\tan\theta}{a} u_g' \bar{v}_g \right.}_{T_3} + \underbrace{\frac{\partial}{\partial \theta} \left(\frac{u_g'}{a} \frac{\partial \bar{v}_g}{\partial \lambda} \right.}_{T_4} + \underbrace{\frac{\partial}{\partial \theta} \left(\frac{\cos\theta}{a} v_g' \frac{\partial \bar{v}_g}{\partial \theta} \right.}_{T_5} + \underbrace{\frac{\partial}{\partial \theta} \left(\frac{\sin\theta}{a} u_g' \bar{u}_g \right.}_{T_6} \right), \tag{4.45}$$

where we use the same T notation to represent the terms in (4.45). We again represent $h', \bar{u}_g$ and $\bar{v}_g$ by h, u_g and v_g respectively. The first term, T_1, is

$$T_1 = \frac{1}{a \cos\theta} \frac{\partial}{\partial \lambda} \left(-\frac{g}{af} \frac{\partial h}{\partial \theta} \frac{\partial u_g}{\partial \lambda} \right. = -\frac{g}{a^2 f \cos\theta} \left(\frac{\partial^2 h}{\partial \lambda \partial \theta} \frac{\partial u_g}{\partial \lambda} + \frac{\partial h}{\partial \theta} \frac{\partial^2 u_g}{\partial \lambda^2} \right. . \tag{4.46}$$

The second term, T_2, becomes

$$T_2 = \frac{\partial}{\partial \lambda} \left(\frac{g}{a^2 f \cos\theta} \frac{\partial h}{\partial \lambda} \frac{\partial u_g}{\partial \theta} \right. = \frac{g}{a^2 f \cos\theta} \left(\frac{\partial^2 h}{\partial \lambda^2} \frac{\partial u_g}{\partial \theta} + \frac{\partial h}{\partial \lambda} \frac{\partial^2 u_g}{\partial \theta \partial \lambda} \right. . \tag{4.47}$$

The third term, T_3, is

$$T_3 = \frac{\partial}{\partial \lambda} \left(\frac{g \tan\theta}{a^2 f} \frac{\partial h}{\partial \theta} v_g \right. = \frac{g \tan\theta}{a^2 f} \left(\frac{\partial^2 h}{\partial \theta \partial \lambda} v_g + \frac{\partial h}{\partial \theta} \frac{\partial v_g}{\partial \lambda} \right. . \tag{4.48}$$

The fourth term, T_4, becomes

$$T_4 = -\frac{\partial}{\partial \theta} \left(\frac{g}{a^2 f} \frac{\partial h}{\partial \theta} \frac{\partial v_g}{\partial \lambda} \right. = -\frac{g}{a^2 f} \left(\frac{\partial^2 h}{\partial \theta^2} \frac{\partial v_g}{\partial \lambda} + \frac{\partial h}{\partial \theta} \frac{\partial^2 v_g}{\partial \theta \partial \lambda} \right. - \frac{g \Gamma_1}{a^2} \frac{\partial h}{\partial \theta} \frac{\partial v_g}{\partial \lambda} . \tag{4.49}$$

The fifth term, T_5, at the moment, is

$$T_5 = \frac{\partial}{\partial\theta}\left(\frac{g}{a^2 f}\frac{\partial h}{\partial\lambda}\frac{\partial v_g}{\partial\theta} \right. = \frac{g}{a^2 f}\left(\right.$$

We now consider the second line of (4.27), where we have ∇f^{-1}. As f is only a function of θ we have the vector $\nabla f^{-1} = (0, \Gamma_1, 0)^T$. Therefore

$$\mathbf{k} \cdot \nabla \left(\frac{\alpha}{f} \quad \times \left(- \right. \right.$$

for h when $\alpha = 0$ and (4.55) with α replaced with 1. This gives two elliptic equations whose solutions are balanced increments to the height field.

We now consider a different method of using the balanced wind field to derive an equation for the balanced height increment where instead of using the relative vorticity we now consider the potential vorticity.

4.3.3 Potential Vorticity Approach (PV)

In this section we derive a generalised version of the balance equation from the potential vorticity of shallow water equations model. The resulting elliptic partial differential equation is a variable coefficient Helmholtz equation. We then find the specific form of the equation for $\alpha = 0$ and $\alpha = 1$.

We start b6ev

then gives us a base state for ξ^c. This is denoted by $\bar{\xi}^c$. We apply the same linearisation to the height field, $h = \bar{h} + h'$, and we still have $\mathbf{u}^{c\prime}$ defined by (4.24), but $\bar{\mathbf{u}}^c$ is defined by

$$\bar{\mathbf{u}}^c \equiv \bar{\mathbf{u}}_g + \frac{2\alpha}{f}\bar{\mathbf{u}}_g \cdot \nabla \left(\mathbf{k} \times \bar{\mathbf{u}}_g\right). \tag{4.59}$$

This is written in component form as

$$\bar{u}^c \equiv \bar{u}_g - \frac{2\alpha}{f}\left(\frac{\bar{u}_g}{a\cos\theta}\frac{\partial \bar{v}_g}{\partial \lambda} + \frac{\bar{v}_g}{a}\frac{\partial \bar{v}_g}{\partial \theta} + \frac{\tan\theta}{a}\bar{u}_g^2 \right. \quad , \tag{4.60}$$

$$\bar{v}^c \equiv \bar{v}_g + \frac{2\alpha}{f}\left(\frac{\bar{u}_g}{a\cos\theta}\frac{\partial \bar{u}_g}{\partial \lambda} + \frac{\bar{v}_g}{a}\frac{\partial \bar{u}_g}{\partial \theta} - \frac{\tan\theta}{a}\bar{u}_g\bar{v}_g \right. \quad . \tag{4.61}$$

In the next step we follow standard procedures for linearisation

$$Q^{c\prime} = f + \mathbf{k} \cdot \nabla \times (^{-}$$

The right hand side of (4.64) is a variable coefficient Helmholtz equation for the balanced height increment, h'.

To complete the balance equation we require a linearisation to the left hand side of (4.57) as we use this to approximate the balanced PV. We achieve this by introducing a linearisation to the full wind, $\mathbf{u} = \bar{\mathbf{u}} + \mathbf{u}'$. This then enables us to linearise the relative vorticity as

$$\xi \equiv \mathbf{k}$$

$$+ \quad 2\cos\theta \frac{\partial \bar{v}_g}{\partial \lambda} \frac{\partial \bar{u}_g}{\partial \theta} - 4\sin\theta \bar{v}_g \frac{\partial \bar{u}_g}{\partial \lambda} + \Big($$

4.4 Alternative Control Variables

In this section we briefly describe the transforms that are currently used to move between the state variables and the control variables before we describe an alternative set of control variables and transforms using h' as the balanced variable.

4.4.1 Current T and U Transforms

The current set of control variables used at the Met Office are comprised of a streamfunction, ψ, velocity potential, χ, and an unbalanced pressure, ${}^{A}P$. In this section we explain the current transforms from the model variable to the control variables, (T transform), and the transform from the control variables back to the model variables, (U transform).

We start with a brief description of the main aim of an incremental 3D VAR scheme. This is to minimise the following cost functional

$$\begin{aligned} J(\delta\mathbf{x}) = &(\delta\mathbf{x} - \delta\mathbf{x}^b)^T \quad \mathrm{B}^{-1} \quad (\delta\mathbf{x} - \delta\mathbf{x}^b) \\ &+ (\boldsymbol{y} - \mathrm{H}(\delta\mathbf{x}))^T \quad \mathrm{R}^{-1} \quad (\boldsymbol{y} - \mathrm{H}(\delta\mathbf{x})), \end{aligned} \tag{4.69}$$

where $\delta\mathbf{x}$ is the increment to the model state vector, $\delta\mathbf{x}^b$ are the increments to a background states, $\boldsymbol{y}$ is the vector of observations, H is an interpolation operator, B is the background error covariance matrix and R is the observation error covariance matrix.

Currently, the model at the Met Office uses around 10^7 model variables across the whole grid and around 10^6 observations. Therefore the two inverse matrices in (4.69) are large and full, although they are never stored.

One advantage of the T transform is it allows a simplification to be made to B. It transforms the matrix into block diagonal as the three control variables are assumed to be uncorrelated, [54]. This then makes the minimisation problem

$$\begin{aligned} J(\delta\mathbf{z}) = (\delta\mathbf{z} - \delta\mathbf{z}^b)^T \quad & \hat{\mathrm{B}}^{-1} \quad (\delta\mathbf{z} - \delta\mathbf{z}^b) \\ + (\boldsymbol{y} - \mathrm{H}(T\delta\mathbf{z}))^T \quad & \mathrm{R}^{-1} \quad (\boldsymbol{y} - \mathrm{H}(T\delta\mathbf{z})), \end{aligned} \tag{4.70}$$

where we have applied a transform matrix, T, such that $\mathbf{z} = T\mathbf{x}$ and this gives $\delta\mathbf{z} = T\delta\mathbf{x}$, $\delta\mathbf{z}^b = T\delta\mathbf{x}^b$ and $\hat{\mathrm{B}} = T\mathrm{B}T^T$.

The current T transform is defined as follows to calculate the stream-function and velocity potential increments, where we shall now use the prime notation that we have used for increment in the thesis so far,

$$\xi' = \nabla \times \mathbf{u}' = \nabla^2\psi', \tag{4.71}$$

$$\delta' = \nabla \cdot \mathbf{u}' = \nabla^2\chi'. \tag{4.72}$$

The transform to calculate the unbalanced pressure involves the solution of a linear balance equation, [54], and statistical regression which we shall not go into here.

The in

model. We also summarised the significant results from the work by Salmon and McIntyre and Roulstone and the definition of the balanced wind field, (3.61), the work in this thesis is based on.

After the summary we briefly derived the SWE for the sphere, (4.1), (4.2) and (4.3) in Section 4.1.1, where we also reviewed a derivation of a spherical non-linear balance equation, [22], which is (4.10).

In Section 4.2 we derived the spherical version of the balanced wind field, (4.12) and (4.13) based on (3.61). It is from these that we derived a spherical

We then extended this idea to a PV approach in Section 4.3.3. We started from the PV equation, (4.57), and through the substitution of a linearisation to ξ^c as $\xi^c = \bar{\xi}^c + \xi^{c\prime}$ which arises from a linearisation to the height field, $h = \bar{h} + h'$. The final equation is (4.67).

In the last section, Section 4.4, we gave a brief description of the current control variable transform, (4.71) and (4.72) and briefly explained the 3D VAR scheme's cost functional.

In Section 4.4.2 we described an alternative to the T transform using (4.55) or (4.67) to calculate the balanced variable, where the two unbalanced variables could be calculated from (4.75) and (4.76). The alternative U transforms were (4.25), (4.26) and (4.73) (evaluated with $\psi^{s\prime}$ and $\chi^{s\prime}$).

In the next c

hapter 5

Ellipticity Theory

In Chapter 4 we derived two new generalised balance equations whose solutions are a balanced height increment. The first equation, (4.55)

$$\xi' = \frac{g}{f}\nabla^2 h' - \frac{2\alpha g}{a^3 f^2 \cos^2\theta}\left(2u_{g\lambda}h_{\theta\lambda} + \cos\theta v_{g\lambda}h_{\theta\theta} - u_{g\theta}h_{\lambda\lambda}\right.$$
$$+2\tan\theta u_{g\lambda}h_\lambda - \cos\theta v_g h_\lambda - 2\tan\theta\sin\theta v_g h_\lambda - 2\sin\theta v_g h_{\theta\lambda} + \cos^2\theta u_g h_\theta$$
$$\left. + \sin\theta\cos\theta\left(u_{g\theta}h_\theta + u_g h_{\theta\theta}\right)\right). \qquad (5.1)$$

is for the relative vorticity method and (4.67)

$$\frac{\xi'}{\bar{h}} - \frac{f+\bar{\xi}}{\bar{h}^2}h'_f = \frac{\xi^{c\prime}}{\bar{h}} - \frac{\left(f+\bar{\xi}^c\right)}{\bar{h}^2}h', \qquad (5.2)$$

is for the potential vorticity method. If we consider (5.1) then we havθ,$\delta\psi\lambda$ *the w e hatha*

(5.2) then α is implicit in the $\xi^{c\prime}$ and $\bar{\xi}^{c\prime}$ terms. For either value of α, 0 or 1, the resulting equation is a variable coefficient Helmholtz equation. All four of these equations are boundary value problems and as such there is a large amount of theory associated with these types of equation, [8], [10], [11], [16], [23], [32], [46].

In Section 5.1 we briefly begin by explaining the spherical grid and the choices for the boundary conditions, we then go on to introduce the theory for the continuous problem by first defining what is meant by an elliptic differential operator and then state the theorem that allows for a solution to exist. This theorem is dependent on the ***ellipticity condition*** which we introduce in Section 5.1.2. We have seen this for the non-linear case (Section 3.3.3) but we now introduce the linear version in Section 5.1.2.

We then derive the ellipticity condition for the four new balance equations in Section 5.1.3. This condition has a significant effect on the equations and many meteorologists have looked for a link between certain flows in the atmosphere and this condition, [25], [26] and [33].

We start Section 5.2 with a brief description of the Met Office's shallow water model from which we generate the base state data. In Section 5.2.2 we describe the numerical approximation that we use to solve (5.1) and (5.2) and we also introduce the theory for discrete elliptic equations.

In the final section, 5.3, we start with a description of the experiments

for which we show results in Chapters 6 and 7. The first is to investigate the structure of the ellipticity condition and the coefficients of the discrete equations. The second is to see the difference between the solutions to the balanced equations. We also describe experiments associated with the assumption that under constant f then the geostrophic wind is non-divergent and the higher order balance, $\mathbf{u}^{c\prime}$ is not divergence free.

To start the shallow water equation model that is described in Section 5.2.1, we use a Rossby-Haurwitz wave and we introduce this in Section 5.3.2. In Section 5.3.3 we introduce three test cases that describe three different Burger regimes. We begin with a summary of the four new balance equations with which the remainder of the thesis is con–i–shba-c¯8bth cothehbIn–free.wD¯–e(weweew

with the equations. The theorem for the existence of the elliptic equation which introduces the ellipticity condition for linear pdes is given in Section 5.1.2, and we examine this condition for the four balance equations in Section 5.1.3.

5.1.1 Balance Equations and Boundary Conditions

As we mention in Chapter 4, the four balance relations are all boundary value problems but so far we have not mentioned the boundary conditions associated with the equations. If we consider the following two diagrams of the domains, (Figures 5.1 and 5.2), we see that the boundary condition for the λ axis is periodicity, but the θ directional boundary condition poses a problem.

The same condition that we use for the λ direction is a possible choice for the two θ boundaries. However, as we cross the poles we change direction. If we consider the direction that the $\mathbf{j}$ unit vector is pointing in as we enter the northern pole then the values of θ are increasing, but as we cross the pole the values of θ are now decreasing.

Another boundary condition is the information that there cannot be a λ derivative at either of the poles due to the singularity there, i.e. all the lines of latitude coincide there, but there is no change in the longitudinal direction

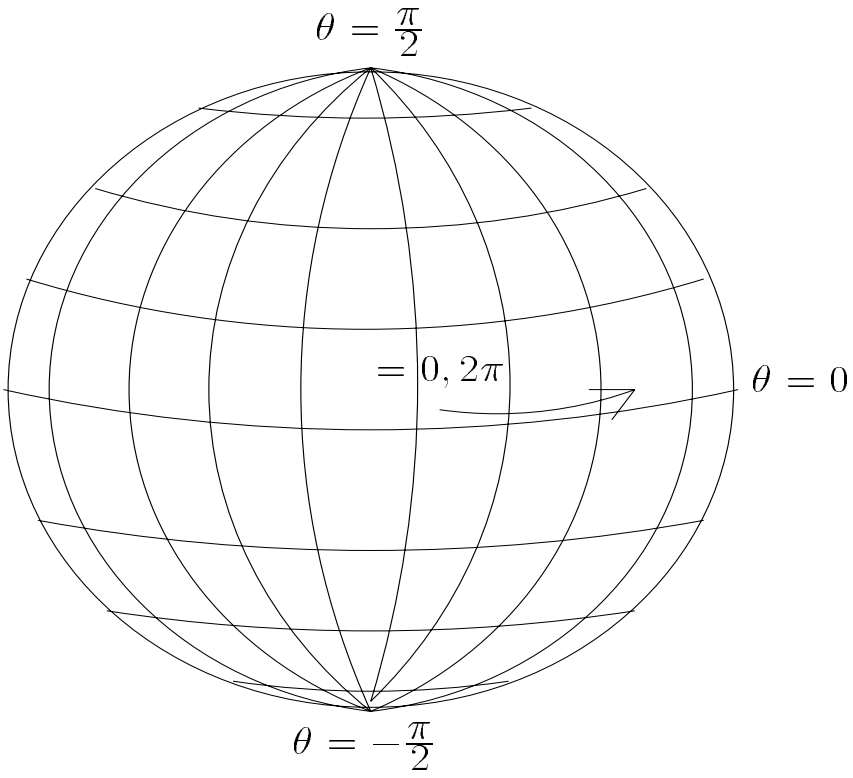

Figure 5.1: Diagram of the Spherical Domain.

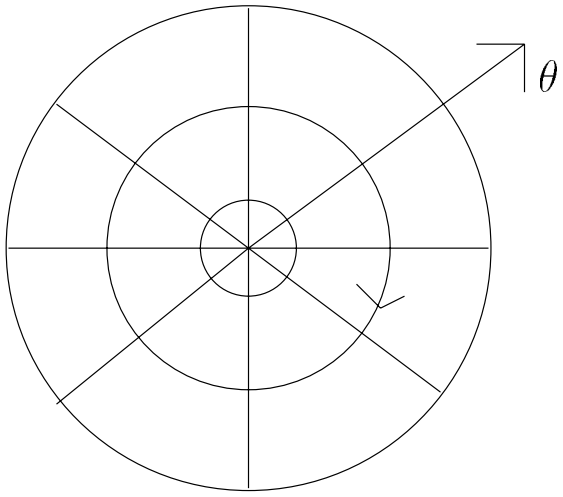

Figure 5.2: Diagram Sho

(see Figure 5.2).

A straightforward condition, for the two poles, is a Dirichlet condition. If we were considering a simple Poisson equation then there is a proof in [46]

Definition 1 *A pde of the form*

$$AS_{\lambda\lambda} + BS_{\lambda\theta} + CS_{\theta\theta} + DS_{\lambda} + \quad S_{\theta} + FS = G, \tag{5.4}$$

where the coefficients, $A, \ldots, G$ *are functions of* θ *and* λ*, is* ***hyperbolic*** *if* $B^2 - 4AC > 0$*,* ***parabolic*** *if* $B^2 - 4AC = 0$ *and* ***elliptic*** *if* $B^2 - 4AC < 0$*.*

This then enables the following definition for the operator to be elliptic.

Definition 2 *The differential operator*

$$L[S] \equiv AS_{\lambda\lambda} + BS_{\lambda\theta} + CS_{\theta\theta}, \tag{5.5}$$

is elliptic if and only if $B^2 - 4AC < 0$*.*

We now give a specific version of a theorem from [11], that defines the existence and uniqueness of the solution to a homogenous elliptic problem.

Theorem 2 *Given the elliptic operator,* $L[S]$*, then the differential equation*

$$L[S] + DS_{\lambda} + \quad S_{\theta} + FS = 0 \tag{5.6}$$

has one solution which has continuous derivatives up to second order in the interior of the domain and is continuous throughout the interior and the boundaries and assumes the prescribed boundary conditions values on the boundary.

The more specific theorem is giv

Definition 3 *The pde, (5.3) is said to be* ***semi-linear*** *if A, B and C are only functions of the independent variables and* ***quasi-linear*** *if the same coefficients are functions of the independent variables and S, S_θ or S_λ.*

Therefore the three balance relations, (5.1) with $\alpha = 1$ and both values for α in (5.2), are semi-linear where the Poisson equation is linear.

The inequality, $B^2 - 4AC < 0$ in definition 1 is the ***ellipticity conditions*** as they are the conditions that ensures that the differential equation has complex characteristics, [11], [16]. This condition is an important propert

For the PV equation, (5.2), then the coefficients for the ellipticity condition are given by

$$A(\theta,\lambda) = \frac{\left(gf + 2\alpha g\frac{\partial \bar{u}_g}{\partial \theta}\right.}{\bar{h}}, \tag{5.15}$$

$$B(\theta,\lambda) = \frac{\left(-4\alpha g\frac{\partial \bar{u}_g}{\partial \lambda} + \frac{4\alpha g\sin\theta}{a}\bar{v}_g\right.}{\bar{h}}, \tag{5.16}$$

$$C(\theta,\lambda) = \frac{\left(gf\cos^2\theta - 2\alpha g\cos\theta\frac{\partial \bar{v}_g}{\partial \lambda} - \frac{2\alpha g\sin\theta\cos\theta}{a}\bar{u}_g\right.}{\bar{h}}. \tag{5.17}$$

This then gives the ellipticity condition coefficients as

$$B^2 = \frac{\alpha^2 16g^2\left(\frac{\partial \bar{u}_g}{\partial \lambda}\right.^2}{\bar{h}^2} - \frac{\alpha^2 32g^2\sin\theta\frac{\partial \bar{u}_g}{\partial \lambda}\bar{v}_g}{a\bar{h}^2} + \frac{\alpha^2 16g^2\sin^2\theta\bar{v}_g^2}{a^2\bar{h}^2}, \tag{5.18}$$

$$\begin{aligned} 4AC = {} & \frac{4g^2f^2\cos^2\theta}{\bar{h}^2} - \frac{\alpha 8g^2 f\cos\theta\frac{\partial \bar{v}_g}{\partial \lambda}}{\bar{h}^2} + \frac{\alpha 8g^2 f\cos^2\theta\frac{\partial \bar{u}_g}{\partial \theta}}{\bar{h}^2} \\ & - \frac{\alpha^2 16g^2\cos\theta\frac{\partial \bar{u}_g}{\partial \theta}\frac{\partial \bar{v}_g}{\partial \lambda}}{\bar{h}^2} - \frac{\alpha^2 16g^2\sin\theta\cos\theta\frac{\partial \bar{u}_g}{\partial \theta}\bar{u}_g}{a\bar{h}^2} \\ & - \frac{8\alpha g^2 f\sin\theta\cos\theta\bar{u}_g}{a\bar{h}^2}. \end{aligned} \tag{5.19}$$

For (5.2) to be elliptic we require (5.18) $<$ (5.19). As with the RV ellipticity condition, (5.13), w

numerical approximation to exist.

5. Numerical Approximations

In the last section we derived the ellipticity conditions for the four balance equations, (5.1) and (5.2) with either $\alpha = 0, 1$. As we see from theorem 2, these are the conditions for the differential equations to have solutions.

In this section we summarise the numerical approximations to (5.1) and (5.2) along with the boundary conditions that we use to calculate the balanced wind field with. We also introduce, in Section 5.2.2, the condition for solutions to the discrete problem to exist.

We start with an introduction to the Met Office's shallow water model that we use to calculate the base states.

5.2.1 Met Office's Shallow Water Model

In this section we briefly introduce the numerical model that we use to calculate the base states. These base states are the three output variables, height, h, zonal wind, u and meridional wind, v.

The grid which the model uses is the Arakawa C-grid, (Figure 5.3). This grid staggers the points, where the height field discrete values are at the points $\Big((j-1)\,\Delta\lambda, -\frac{\pi}{2} + (i-1)\,\Delta\theta\Big)$, with $i = 1, 2, \ldots, N$, $j = 1, 2, \ldots,$,

h_{i+1}

the two time levels. The solution to the Helmholtz problem is obtained through using a multigrid procedure. There is a more detailed description in [28].

5.2.2 Numerical Approximations to the New Balance Equations

In this section we describe the numerical approximations that we use to solve equations (5.1) and (5.2), we also give a description of the approximations to calculate $\mathbf{u}^{c\prime}$.

We shall also summarise the conditions for a solution to the discrete equation to exist; a more detailed description is given in [32] and [46]. We start with a description of the numerical approximations used for the coefficients in the differential equation.

The linearisation factors are the geostrophic winds and their derivatives. We calculate the geostrophic winds from the base height, $\bar{h}$, given in spherical coordinates by (4.22) and (4.23). We approximate these with the central differences

$$u_{g,i,j} \approx -\frac{g}{f_i a}\frac{\bar{h}_{i+1,j}-\bar{h}_{i-1,j}}{2\Delta\theta}, \qquad v_{g,i,j} \approx \frac{g}{a f_i \cos\theta_i}\frac{\bar{h}_{i,j+1}-\bar{h}_{i,j-1}}{2\Delta\lambda}, \qquad (5.21)$$

where $f_i = 2\Omega\sin\theta_i$ and $\theta_i = -\frac{\pi}{2} + (i-1)\,\Delta\theta$. These approximations are second order,[32], [46] and consistent with (4.22) and (4.23), [1] and [23].

To enforce the periodicity condition in the λ direction we use the conditions that for the points $j =$ then $j + 1 = 1$ and for the points $j = 1$ then $j - 1 =$. At the two θ boundaries, we use the periodicity condition to approximate $(i + 1, j)$ at the north pole with $\left(i - 1, j + \frac{}{2}\right)$ for $j \leq \frac{}{2}$ and $\left(i - 1, j - \frac{}{2}\right)$ for $\frac{}{2} < j \leq$. For the south pole it is the $(i - 1, j)$ term that is approximated. Then for $(i - 1, j)$ this is $\left(i - 1, j + \frac{}{2}\right)$ for $j \leq \frac{}{2}$ and $(i - 1, j)$ is $\left(i + 1, j - \frac{}{2}\right)$ for $\frac{}{2} < j \leq$.

For the numerical experiments we perform in Chapters 6 and 7 we have taken $= 96$ and $N = 65$.

To calculate the first derivatives of the geostrophic winds we apply the central differences

$$\frac{\partial \bar{u}_g}{}$$

are given by

$$\frac{\partial^2 h'}{\partial \lambda^2} \approx \frac{h'_{i,j+1} - 2h'_{i,j} + h'_{i,j-1}}{a^2 \Delta \lambda^2}, \qquad \frac{\partial^2 h'}{\partial \theta^2} \approx \frac{h'_{i+1,j} - 2h'_{i,j} + h'_{i-1,j}}{a^2 \Delta \theta^2}. \quad (5.24)$$

where for the λ direction we use a periodicity condition and apply this the same way as for the geostrophic wind calculations. These can be shown to be a second order approximation, [46], [32], and also consistent, [1], [23].

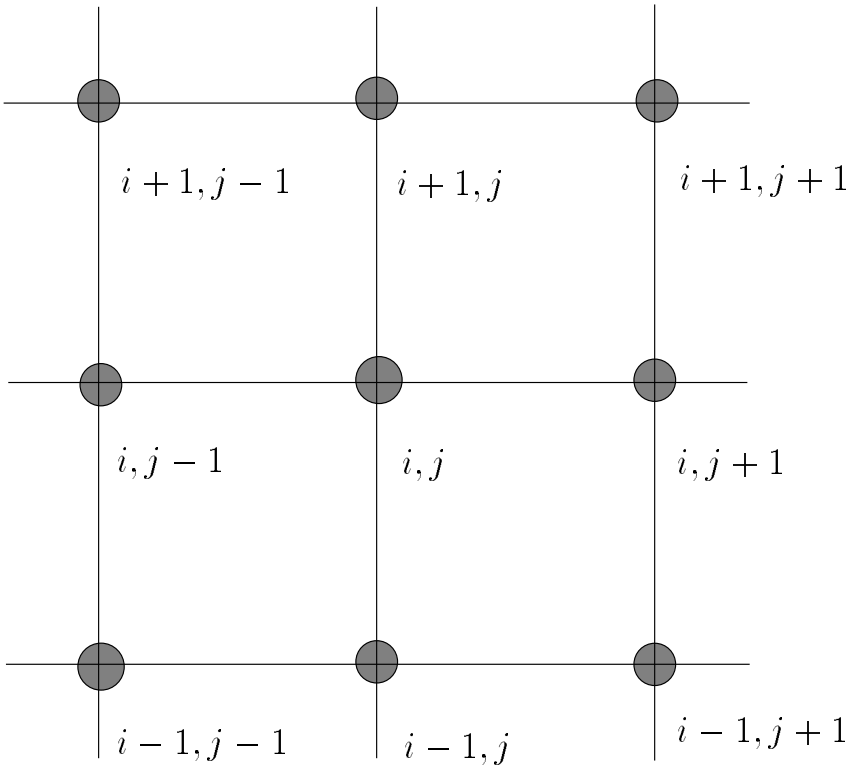

Figure 5.4: Diagram of the Nine-Point Stencil.

The cross derivative approximation is derived as follows

$$\begin{aligned} \frac{\partial^2 h'}{\partial \theta \partial \lambda} &\approx \frac{1}{2\Delta\theta} \left(\frac{h'_{i+1,j+1} - h'_{i+1,j-1}}{2\Delta\lambda} - \frac{h'_{i-1,j+1} - h'_{i-1.j-1}}{2\Delta\lambda} \right), \\ &\approx \frac{h'_{i+1,j+1} + h'_{i-1,j-1} - h'_{i+1,j-1} - h'_{i-1,j+1}}{4\Delta\theta\Delta\lambda}. \end{aligned} \quad (5.25)$$

It is this last approximation that makes the numerical approximate to the differential equation into a nine-point stencil, as we use the four corner points in Figure 5.4.

To complete the discrete approximation to equations (5.1) and (5.2) we require approximations for $\bar{\xi}^c$ and $\xi^{c\prime}$. We use the full relative vorticity, ξ, and calculate $\bar{\xi} = \mathbf{k} \cdot \nabla \times \bar{\mathbf{u}}$, with $\xi' = \xi - \bar{\xi}$, and $\bar{\mathbf{u}}$ is the base state wind field.

We require ξ' at the h points in the grid but this variable is dependent on the derivatives of the wind fields which are not evaluated at the h points. We overcome this by using the following approximation which is second order in the horizontal directions, [57].

$$
\begin{aligned}
\xi'_{i,j} &\approx \left(\mathbf{k} \cdot \nabla \times \mathbf{u}'_{i,j}\right), \qquad (5.26)\\
&\approx \frac{1}{a\cos\theta}\left(\frac{\partial v'}{\partial \lambda} - \frac{\partial}{\partial \theta}\left(\cos\theta u'\right)\right)_{i,j},\\
&\approx \frac{1}{a\cos\theta_i}\left(\frac{v'_{i,j+1} - v'_{i,j-1} + v'_{i-1,j+1} - v'_{i-1,j-1}}{4\Delta\lambda}\right.\\
&\quad \left. - \cos\theta_{i+1}\left(u'_{i+1,j} + u'_{i+1,j-1}\right) - \cos\theta_{i-1}\left(u'_{i-1,j} + u'_{i-1,j-1}\right)\right)
\end{aligned}
$$

2. *A is diagonally dominant and strictly diagonally dominant for at least one row,*

3. *A is irreducible.*

This then leads to the following theorem, [51].

Theorem 3 *If the matrix A is a M-Matrix, then it is invertible.*

Therefore if the matrix that arises from the discretisation of the elliptic pde satisfies these conditions then there exist a solution.

The final set of numerical approximations we derive concern $\mathbf{u}^{c\prime}$. Once we have solved the discrete elliptic equation we have a *balanced* height increment but to calculate the other two control variables, $\psi^{s\prime}$ and $\chi^{s\prime}$, (Section 4.4), we have to calculate the velocity split, (4.74), and so we have to calculate $\mathbf{u}^{c\prime}$ from the height, (4.24) i.e. we have to numerically approximate (4.25) and (4.26). To do this we have to calculate both the base state and incremental geostrophic wind, $\bar{u}_g, \bar{v}_g, u'_g$ and v'_g at the u, v points, along with their first derivatives.

To do this we follow a similar method that is used to calculate ξ'. We begin with u_g at the u points, where u_g is geostrophic wind. If we follow the approximation for ξ'

To calculate the u_g component at the u points we evaluate the following expression

$$-\frac{1}{a}\frac{\partial h}{\partial \theta}\bigg|_{i,j+\frac{1}{2}} \approx \frac{1}{a}\left(\frac{h_{i-1,j}+h_{i-1,j+1}-(h_{i+1,j+1}+h_{i+1,j})}{4\Delta\theta}\right. \quad . \tag{5.29}$$

If we look at Figure 5.5 we see where the averages lie and how we can use these to calculate u_g at the u points. Here we have used a general height to illustrate that we can apply the same approximation to either $\bar{h}$ or h'.

$h_{i+1,j}$ $\hat{h}_{i+1}$ $h_{i+1,j+1}$

$h_{i,j}$ $u_{i,j}$ $h_{i,j+1}$

$h_{i-1,j}$ $\hat{h}_{i-1}$ $h_{i-1,j+1}$

Figure 5.5: Diagram for the weighting of the u component of the geostrophic wind at the u point, where $\hat{h}_{i+1} = \frac{h_{i+1,j+1}+h_{i+1,j}}{2}$ and $\hat{h}_{i-1} = \frac{h_{i-1,j+1}+h_{i-1,j}}{2}$.

To calculate the v_g component at the u point we use

$$\frac{1}{a\cos\theta}\frac{\partial h}{\partial \lambda}\bigg|_{i,j+\frac{1}{2}} \approx \frac{1}{a\cos\theta_i}\left(\frac{h_{i,j+1}+h_{i,j+2}-(h_{i,j}+h_{i,j-1})}{4\Delta\lambda}\right. \quad . \tag{5.30}$$

We have drawn a diagram to show where the averages lie for this approximation, Figure 5.6. For the two geostrophic winds to be evaluated at the v

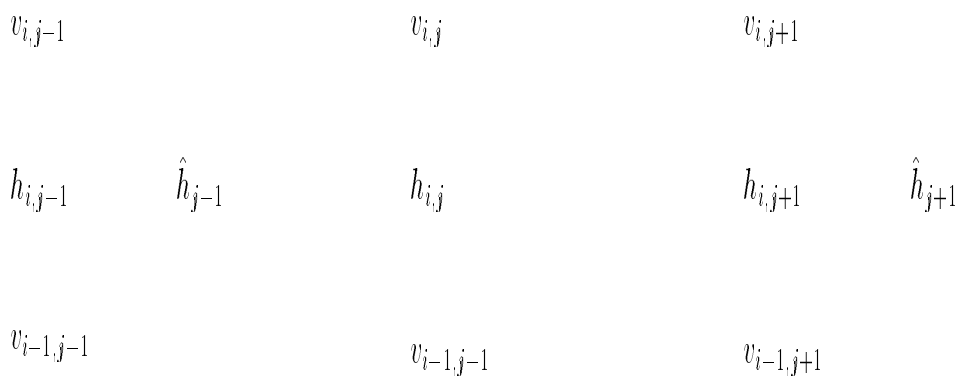

Figure 5.6: Diagram for the weighting of the v component of the geostrophic wind at the u point where $\hat{h}_{j+1} = \frac{h_{i,j+1} + h_{i,j+2}}{2}$ and $\hat{h}_{j-1} = \frac{h_{i,j-1} + h_{i,j}}{2}$.

points we use the following expression (see also the diagrams of the approximations in Figures 5.7 and 5.8)

$$-\frac{1}{a}\frac{\partial h}{\partial \theta}\bigg|_{i+\frac{1}{2},j} \approx -\frac{1}{a}\left(\frac{h_{i+1,j} + h_{i,j} - h_{i-1,j} - h_{i-2,j}}{4\Delta\theta}\right. , \tag{5.31}$$

$$\frac{1}{a\cos\theta}\frac{\partial h}{\partial \lambda}\bigg|_{i+\frac{1}{2},j} \approx \frac{1}{a\cos\theta_{i+\frac{1}{2}}}\left(\frac{h_{i,j-1} + h_{i-1,j-1} - h_{i,j+1} - h_{i-1,j+1}}{4\Delta\lambda}\right. . \tag{5.32}$$

This completes all the numerical approximations we use to calculate h',

δ

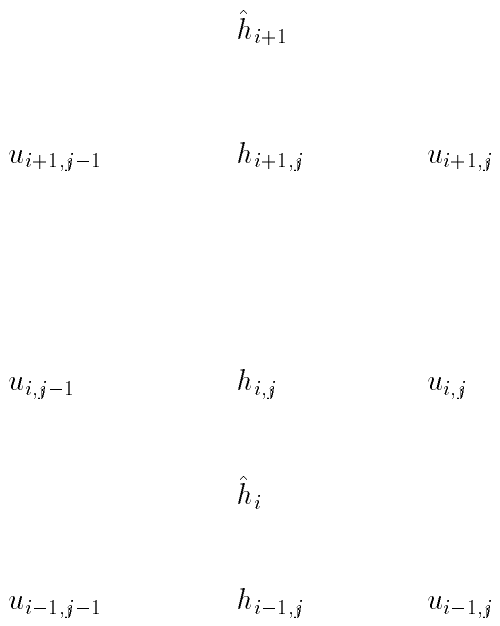

Figure 5.7: Diagram for the weighting of the u component of the geostrophic wind at the v point where $\hat{h}_{i+1} = \frac{h_{i+2,j} + h_{i+1,j}}{2}$ and $\hat{h}_i = \frac{h_{i,j} + h_{i-1,j}}{2}$.

$h_{i+1,j-1}$ $h_{i+1,j}$ $h_{i+1,j+1}$

5.3 Initial Conditions

In this section we describe briefly in 5.3.1 the experiments that we perform using the data generated from the shallow water model. Then in Section 5.3.2 we introduce the Rossby-Haurwitz wave. This wave is the initial condition that we use to generate different types of flow regimes in the SWE model. In Section 5.3.3 we introduce three test cases that arise from varying certain parameters in the Rossby-Haurwitz wave. This then generates different Burger number regimes, which we also introduce in this section.

5.3.1 Experiments

There are four sets of experiments that we perform involving the four balance equations. The first experiment involves evaluating the ellipticity condition for (5.1) and (5.2) with $\alpha = 1$, for three test cases both at the initial time and at 72 hrs into the model run. At both time levels we compare the condition to that of the equations when $\alpha = 0$.

The second set involves a scale analysis at $\theta = 45°N$ of the terms in the ellipticity conditions and the coefficients of the differential equation to see if there are any terms that could be removed to make the solution of the numerical equation more economical.

The other two experiments, the results of which are presented in Chapter

7, are concerned with the numerical solutions of the four balance relations on the sphere for the same three test cases. We look at $\|\boldsymbol{b}\|_2 = \sqrt{\sum_{i\ 1}^{N} b_i^2}$ where $\boldsymbol{b}$ is a general vector and b_i is a general entry in $\boldsymbol{b}$. For our experiment we form a vector for each latitudinal ring of the difference between the full height increment, h'_f, and the balanced height increment, h', in the mid-latitudes to see how each method differs in the different Burger regimes. The last experiment involves testing the hypothesis that for constant f the new balanced wind field is divergent.

5.3.2 Rossby Haurwitz Wave

The Rossby-Haurwitz wave was shown to be an analytical solution to the non-linear barotropic vorticity equation on the sphere by Haurwitz [18]. The equation for the barotropic vorticity model is

$$\frac{\partial \zeta}{\partial t} + (\mathbf{u} \cdot \nabla)\, \zeta = 0, \tag{5.33}$$

with

$$\boldsymbol{u} = \quad \times \nabla \psi, \qquad \zeta = \quad . \nabla \times \boldsymbol{u} = \nabla^2 \psi.$$

A solution to this differential equation is of the following form

$$\psi = -a^2 \omega \sin\theta + K \cos^R \theta \sin\theta \cos R\lambda, \tag{5.34}$$

where $A(\theta), B(\theta)$ and $C(\theta)$ are given by

$$A(\theta) = \frac{\omega}{2}(2\Omega + \omega$$

tions we define the *Burger number*, [5], [6], B_u, given by

$$B_u \equiv \frac{\sqrt{gh}}{fL} = \frac{L_R}{L}, \tag{5.42}$$

where L_R is the Rossby radius of deformation. As we can see from (5.42), as we approach the equator, $\theta = 0$, then $f \to 0$ and so $B_u \to \infty$. The three test cases that we consider generate different values for B_u at different latitudinal levels.

As we mentioned in Section 2.1, it is often assumed that the atmospheric motions in the horizontal directions are larger than those in the vertical. A result of this is that the atmosphere can be considered as a number of layers of fluid. A fluid with this property is said to be stably stratisfied, [34]. The Burger number describes the relative importance bet

$10^{-7}s^{-1}$. The second test case, (TC2), is defined to be $h_0 = 8000m$, $\omega = K = 7.848 \times 10^{-6}s^{-1}$. The third test case, (TC3), is defined to be $h_0 = 8000m$, $\omega = K = 7.848 \times 10^{-7}s^{-1}$. For the initial heigh

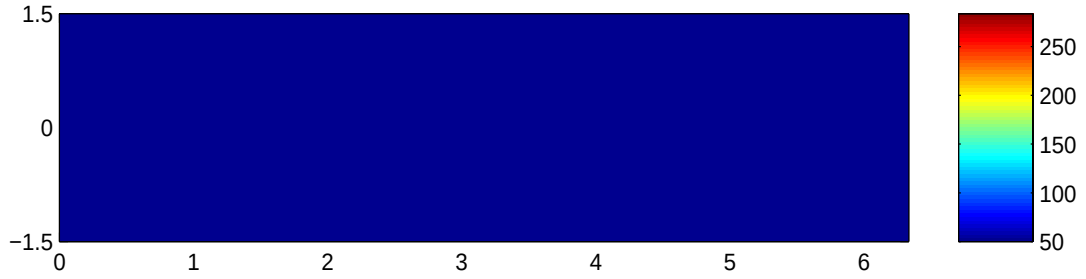
1.5
0
−1.5
0
1
2
3
4
5
6
250
200
150
100
50

equations.

In Section 5.2 we gave a brief description of the shallow water equations model that we use to generate the base state data. Also in this section we gave a description of the numerical approximations that w

hapter 6

Ellipticity Experiments

In this chapter we explain and present results from experiments on the ellipticity conditions for the two equations (5.1) and (5.2).

We describe the experiments that we perform on the ellipticity condition in Section 6.1. The first set of experiments are concerned with the initial heights for the three test cases. As we require the geostrophic winds, calculated from the height fields, we have to calculate the derivatives of the height field. In Section 6.2 we describe how we calculate these derivatives for both the initial height profile and the height at 72hrs. At the initial time we use the continuous expression for the height and the derivatives are explained in Section 6.2.1. For the experiments at 72hrs we only have the numerical values for the height rather than the continuous expressions and as such we describe the procedure to approximate the derivatives in Section 6.2.2.

72hrs into the run of the SWE model with the three test cases. To calculate the coefficients for this experiment we use the numerical approximations explained in Section 5.2.2.

In both experiments we compare the ellipticity plots with the equivalent condition for the case where $\alpha = 0$, geostrophic balance. For the RV method this is simply a set of increasingly valued parallel lines as we enter the equatorial regions. This is not the case for the PV method and we present the condition for the PV method in separate plots for all three test cases.

We also introduce a fourth test case that fails the ellipticity condition, which shows that the ellipticity condition will not be satisfied by unphysical data.

We then repeat the plots for the three test cases at 72 hours into the 120 hour run of the shallow water model. Here we see how the condition is affected by the slanting in the waves and the movement of the height field.

Another objective of this research is to see whether or not we need to calculate all the terms in the equation. To do this we perform a scale analysis using values from each of the three test cases for the mid-latitudes. We apply this to both the coefficients in the ellipticity condition and the coefficients in the differential equations, (5.1) and (5.2). The reason for this is both equations contain many lower order differential terms that may be very small.

6. Calculations of the Ellipticity Condition's Coefficients

As we described in Section 6.1, we perform experiments on the coefficients of the ellipticity condition and the discrete and continuous elliptic differential equations that we derived in Chapters 4 and 5. In this section we briefly explain how we evaluate the coefficients. We start with the continuous coefficients in Section 6.2.1 and then briefly recall the expression for the derivatives from Section 5.2.2 in Section 6.2.2.

6.2.1 Continuous Coefficients Calculations

If we recall the expression that we gave in Section 5.3.2 for the initial height profile for a Rossby-Haurwitz wave, (5.35)

$$h = \frac{1}{g}\left\{gh_0 + a^2A(\theta) + a^2B(\theta)\cos R\lambda + a^2C(\theta)\cos 2R\lambda\right\},$$

where A, B and C are given by (5.39), (5.40) and (5.41) respectively, then to calculate the geostrophic winds we require the first derivatives of (5.35) with respect to both θ and λ. This is therefore

$$\frac{\partial h}{\partial \lambda} = \frac{1}{g}\left(-Ra^2B(\theta)\sin R\lambda - 2Ra^2C(\theta)\sin 2R\lambda\right), \quad (6.1)$$

$$\frac{\partial h}{\partial \theta} = \frac{1}{g}\left(a^2\frac{\partial A(\theta)}{\partial \theta} + a^2\cos R\lambda\frac{\partial B(\theta)}{\partial \theta} + a^2\cos 2R\lambda\frac{\partial C(\theta)}{\partial \theta}\right), \quad (6.2)$$

where the expressions for the θ derivatives of A, B, and C are in Appendix C. We also require the second derivatives of h and these are given by

We have used the central differences that were described in Section 5.2.2 to approximate the derivatives in the coefficients, (5.7) - (5.9) and (5.15) - (5.17). We therefore evaluate the coefficients of the ellipticity condition at the grid points.

6.3 Results I: Ellipticity Plots

In this section we present discussion for the initial ellipticity condition that has been calculated using the analytical expressions derived in Section 6.2.1.

We present the ellipticity conditions in a series of figures, Figures 6.2 to 6.7 and 6.11 to 6.16. Each figure contains four plots. These show, from top left to bottom right, B^2, $4AC$, $B^2 - 4AC$ and h. We compare the ellipticity plots with the equivalent condition for the Laplacian. For the PV method we present the ellipticity condition for $\alpha = 0$ in Figure 6.1 for $t = 0$ and Figure 6.10 for $t = 72$, and then compare the relevant plot for each test case.

We also give a fourth test case that fails the ellipticity condition. This problem is unphysical, but where the height is unphysical is near where the condition fails.

6.3.1 Initial Ellipticity Conditions

As we have mentioned in the introduction to this section we are to compare the ellipticity plots for each test case against the equivalent condition for the

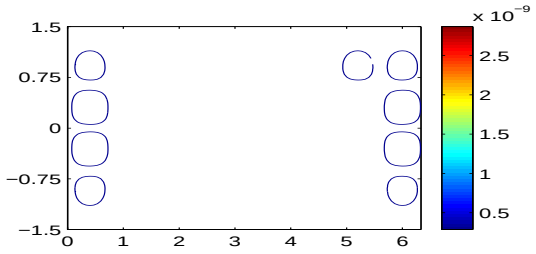
x 10^−9
2.5
2
1.5
1
0.5
1.5
0.75
0
−0.75
−1.5
0
1
2
3
4
5
6

As we can see from the two figures there is a significant difference in the structure in the two ellipticity conditions but both conditions are dominated by the $4AC$ term. We are not surprised by the difference between the two methods' conditions as this is consistent with the findings from [57]. We shall see the consequences of this in Chapter 7.

If we consider the results for the RV method (Figure 6.2) then comparing to a set of parallel lines there would appear a similar structure to this in the mid-latitudes but as we enter the equatorial regions this is not the case. The structure as we enter this region appears similar to that of the wave.

Another feature is the size of the dominance of the $4AC$ term over the B^2 term. For this test case this is 10^3 which is quite a substantial difference but as we can see, the changes in the wave's height profile with respect to the two directions is larger in TC2 than TC1.

A noticeable feature in the PV method's ellipticity condition is the vortitices that are formed in the troughs of the Rossby-Haurwitz wave. In these areas the ellipticity condition is at its most negative possible^^TD^turenegatinTJ^–p–ossibletrofil

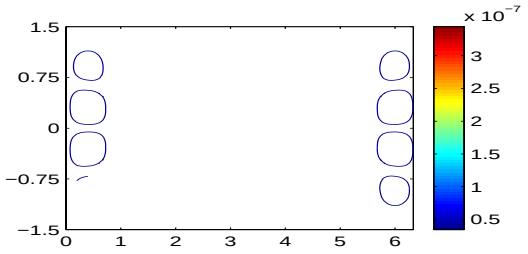
1.5
0.75
0
−0.75
−1.5
0
1
2
3
4
5
6
× 10^−7
3
2.5
2
1.5
1
0.5

The first feature that stands out from Figure 6.4 is that there is nothing resembling the structure of a set of parallel lines. Comparing the PV method's ellipticity condition to its Laplacian equivalent, (top right in Figure 6.1), then this is also suggesting that for this type of flow then the extra terms from taking the higher order balance are essential.

Another striking difference between the results for TC1 and TC2 is the size of the difference between B^2 and $4AC$

wmethbiguisndanfdr–T.hoT^^T–W–wT^^Tthe–ature–A
Comped–wone.

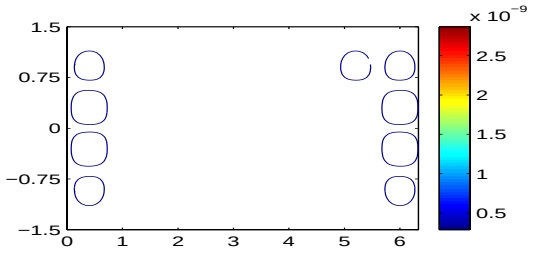
1.5
0.75
0
−0.75
−1.5
0
1
2
3
4
5
6
× 10^−9
2.5
2
1.5
1
0.5

We do not have a change in the structure of the conditions between the RV and PV methods as in TC1. This is again consistent with [57], we go into more details about these findings when we calculate the solutions to the equations in Chapter 7.

As we mentioned in the introduction to this section we have a fourth test case that has the ellipticity condition failing for both methods. For this fourth test case, TC4, is defined by $h_0 = 8000m$, $\omega = K = 7.848 \times 10^{-5} s^{-1}$, the height field is shown in Figure 6.8. The ellipticity plots are in Figure 6.9.

As we can see this is an unphysical example as we can not have negative values for the full height field. The effect this has on the coefficients in the ellipticity conditions is seen in Figure 6.9.

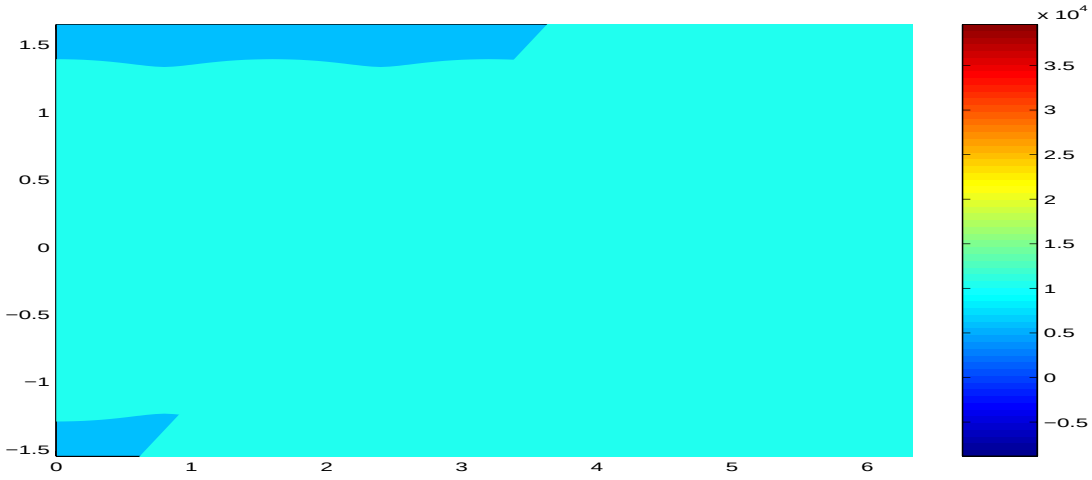

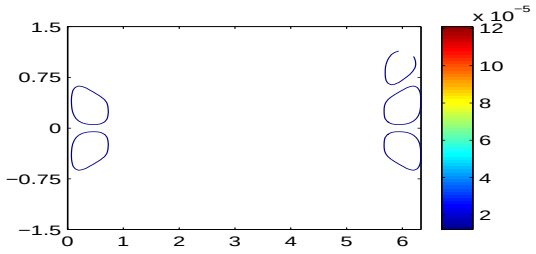
x 10^−5
1.5
0.75
0
−0.75
−1.5
0
1
2
3
4
5
6
12
10
8
6
4
2

also still a noticeable difference between the two methods.

An interesting feature in the plots is the distortion of the B^2 term for

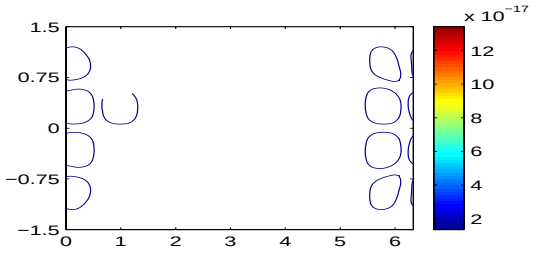
1.5
0.75
0
−0.75
−1.5
0
1
2
3
4
5
6
× 10^−17
12
10
8
6
4
2

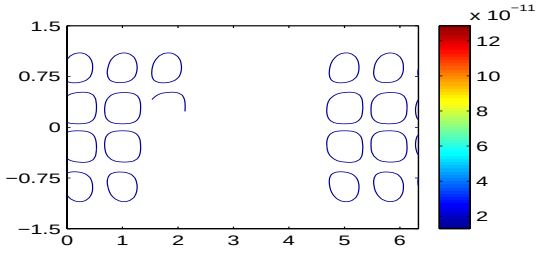
1.5
0.75
0
−0.75
−1.5
0
1
2
3
4
5
6
× 10^−11
12
10
8
6
4
2

test cases at 72 hrs. These are in Table 6.1, where we have taken the value for f at 45°N of $1.0312 \times 10^{-4} s^{-1}$ and $a = 6371220m$

Test Case	$\bar{h}$	$\bar{u}_g$	$\bar{v}_g$	$\frac{\partial \bar{u}_g}{\partial \lambda}$	$\frac{\partial \bar{v}_g}{\partial \lambda}$	$\frac{\partial \bar{u}_g}{\partial \theta}$
1	165.79	3.48	2.73	6.72×10^{-7}	1.69×10^{-6}	1.14×10^{-6}
2	9.10×10^{3}	27.94	26.72	5.83×10^{-6}	1.66×10^{-6}	5.30×10^{-6}
3	8.10×10^{3}	3.65	2.22	6.45×10^{-7}	1.38×10^{-6}	2.78×10^{-7}

Table 6.1: Table of the Average Values for Scale Analysis, where h has units m, $\bar{u}_g$, $\bar{v}_g$ ha$_g$ haψ

altered substantially.

If we were to consider whether or not to remove terms we would have to say that for TC2 we would have to consider not removing any of the terms that make up $4AC$ as these are comparable with the Laplacian term in the mid-latitudes. We would also have to consider leaving all the terms in B^2 as again these are comparable to $4AC$.

For the other two test cases the averaged value for B^2 is not comparable with $4AC$ and as such the removal of the cross derivative terms from the point of view of the ellipticity condition would not affect the condition too severely. For TC1 we could possibly remove the term involving the $\frac{\partial^2 h'}{\partial \lambda^2}$ as the coefficien

Coefficient (ms^{-3})	Term	TC1	TC2	TC3
gf	$h_{\lambda\lambda}$	1.01×10^{-3}	1.01×10^{-3}	1.01×10^{-3}
$\sin\theta\cos\theta fg$	h_{θ}	5.06×10^{-4}	5.06×10^{-4}	5.06×10^{-4}
$\cos^2\theta fg$	$h_{\theta\theta}$	5.06×10^{-4}	5.06×10^{-4}	5.06×10^{-4}
$2g\frac{\partial \bar{u}_g}{\partial \lambda}$	$h_{\theta\lambda}$	2.62×10^{-5}	2.29×10^{-4}	2.53×10^{-5}
$2g\cos\theta\frac{\partial \bar{v}_g}{\partial \lambda}$	$h_{\theta\theta}$	2.34×10^{-5}	2.30×10^{-5}	1.94×10^{-5}
$2g\frac{\partial \bar{u}_g}{\partial \theta}$	$h_{\lambda\lambda}$	2.24×10^{-5}	1.04×10^{-4}	5.45×10^{-6}
$\frac{4g\sin\theta}{a}\bar{v}_g$	$h_{\theta\lambda}$	1.19×10^{-5}	1.16×10^{-4}	9.67×10^{-6}
$\frac{2g\sin\theta\cos\theta}{a}\bar{u}_g$	$h_{\theta\theta}$	5.36×10^{-6}	4.30×10^{-5}	5.62×10^{-6}
$\frac{(4g\tan\theta\sin\theta + 2g\cos\theta)}{a}\bar{v}_g$	h_{λ}	1.78×10^{-5}	1.75×10^{-4}	1.45×10^{-5}
$\frac{2g\cos^2\theta}{a}\bar{u}_g$	h_{θ}	5.36×10^{-6}	4.30×10^{-6}	5.62×10^{-6}
$4g\tan\theta\frac{\partial \bar{u}_g}{\partial \lambda}$	h_{λ}	2.64×10^{-5}	2.29×10^{-4}	2.53×10^{-5}
$2g\sin\theta\cos\theta\frac{\partial \bar{u}_g}{\partial \theta}$	h_{θ}	1.12×10^{-5}	5.20×10^{-5}	2.73×10^{-6}

Table 6.4: Scale Analysis of the Coefficients in the Differential Equation for the RV Method

These are the coefficients that make up the Laplacian operator. For TC1 we see that the extra terms are of a similar scale to the Laplacian, but $O\left(10^{-1}\right)$ smaller. The only terms that are 10^{-2} smaller are those that arise from T_6 in (4.34) and (4.45) and as such for this type of flow we may consider dropping

these terms. One of these coefficients does multiply a second derivative term and as such w

Coefficient (s^{-6})	TC1	TC2	TC3
$\frac{16g^2\left(\frac{\partial \bar{u}_g}{\partial \lambda}\right)^2}{\bar{h}^2}$	2.53×10^{-14}	6.31×10^{-16}	9.73×10^{-18}
$-\frac{32g^2 \sin\theta \frac{\partial \bar{u}_g}{\partial \lambda}\bar{v}_g}{a\bar{h}^2}$	-2.28×10^{-14}	-6.42×10^{-16}	-7.42×10^{-18}
$\frac{16g^2 \sin^2\theta \bar{v}_g^2}{a^2\bar{h}^2}$	5.13×10^{-15}	1.63×10^{-16}	1.42×10^{-18}
B^2	7.63×10^{-15}	1.52×10^{-16}	3.73×10^{-18}

Table 6.5: Scale Analysis of the Coefficients in B^2 for the PV Method

Coefficient β	-	T j - T ^ ^ T f -	^ ^ T D -	^ T c - 6 3 T j - T ^ ^ T f -

for the RV method.

For TC2 we see that the Laplacian term is not dominating this condition but again we have factors in the B^2 term that could not be dropped as for the RV method. This is consistent with the results in Figure 6.14.

The final test case's results are consistent with the RV method's results with the Laplacian being the largest factor in the $4AC$ term. We now consider the whole differential equation to see what lower order terms could also possibly be removed due to their size. The values for the terms are displayed in Table 6.7.

The first feature of the results in Table 6.7 is that the v

Coefficient, s^{-3}	Term	TC1	TC2	TC3
$\dfrac{gf}{\bar{h}}$	$h_{\lambda\lambda}$	6.09×10^{-6}	1.11×10^{-7}	1.25×10^{-7}
$\dfrac{\sin\theta\cos\theta f g}{\bar{h}}$	h_{θ}	3.05×10^{-6}	5.56×10^{-8}	6.24×10^{-8}
$\dfrac{\cos^2\theta f g}{\bar{h}}$	$h_{\theta\theta}$	3.05×10^{-6}	5.55×10^{-8}	6.23×10^{-8}
$\dfrac{2g\dfrac{\partial \bar{u}_g}{\partial\lambda}}{\bar{h}}$	$h_{\lambda\theta}$	1.59×10^{-7}	2.51×10^{-8}	3.12×10^{-9}
$\dfrac{2g\cos\theta\dfrac{\partial \bar{v}_g}{\partial\lambda}}{\bar{h}}$	$h_{\theta\theta}$	1.44×10^{-7}	2.53×10^{-9}	2.36×10^{-9}
$\dfrac{2g\dfrac{\partial \bar{u}_g}{\partial\theta}}{\bar{h}}$	$h_{\lambda\lambda}$	1.35×10^{-7}	1.14×10^{-8}	6.73×10^{-10}
$\dfrac{4g\sin\theta\bar{v}_g}{a\bar{h}}$	$h_{\lambda\theta}$	7.17×10^{-8}	1.28×10^{-8}	1.19×10^{-9}
$\dfrac{2g\sin\theta\cos\theta\bar{u}_g}{a\bar{h}}$	$h_{\theta\theta}$	3.23×10^{-8}	4.73×10^{-9}	6.94×10^{-10}
$\dfrac{(4g\tan\theta\sin\theta + 2g\cos\theta)\,\bar{v}_g}{a\bar{h}}$	h_{λ}	1.08×10^{-7}	1.92×10^{-8}	1.79×10^{-9}
$\dfrac{2g\cos^2\theta\bar{u}_g}{a\bar{h}}$	h_{θ}	3.23×10^{-8}	4.73×10^{-9}	6.94×10^{-10}
$\dfrac{4g\tan\theta\dfrac{\partial \bar{u}_g}{\partial\lambda}}{\bar{h}}$	h_{λ}	1.59×10^{-7}	2.50×10^{-8}	3.12×10^{-9}
$\dfrac{2g\sin\theta\cos\theta\dfrac{\partial \bar{u}_g}{\partial\theta}}{\bar{h}}$	h_{θ}	6.76×10^{-8}	5.71×10^{-9}	3.37×10^{-10}
$a^2 f^2 \cos^2\theta \left(\dfrac{f + \mathbf{k}\cdot\nabla\times\bar{\mathbf{u}}_g^c}{\bar{h}^2} \right.$	ψ$TJ∂theψωtia quatic			

For TC2 we see that the scale of most of the terms in Table 6.7 are comparable with both the Helmholtz and the Laplacian part of the equations. The exception is again the terms arising from T_6 in (4.45). We would then have the same question of the effect that this has if the same term is removed from $\bar{\xi}^c$.

The final test case would appear again to be dominated by the Laplacian but there is an effect from the Helmholtz part. We would have to consider the removal of all the extra terms arising from the higher order terms in the balance relation in $\bar{\xi}^c$. For this flow we have seen that there is a more geostrophic structure to it than the other two and so the same approximation in $\bar{\xi}^c$ should not have too much of an affect.

6.5 Conclusions

The main aim of these experiments that we have shown in this chapter was to try and identify types of flows where we would gain extra information from the new balance equations. We undertook this by considering the initial ellipticit

having some effect as the plots did not look similar to a latitudinal dependent condition. For the PV method then there was some similarity between the full condition and the Laplacian equivalent for TC1.

With the PV method the ellipticity condition changes quite drastically, (Figure 6.4), suggesting that there may be some benefit from using the extra terms in the calculation of $\xi^{c\prime}$ in the PV method. The same structure was still present at 72 hours but had moved with the wave, (Figure 6.12).

For TC2 we saw no structure resembling the ellipticity condition for the Laplacian, (Figure 6.2), which was still true at 72 hours (Figure 6.13) for the RV method. This suggests that the extra terms are needed here to model flows of this type. This was also true for the PV method.

In the plots of the initial ellipticity condition for both the RV and PV methods for TC3 (Figures 6.6 and 6.7) then there was a structure similar to the condition for the Laplacians in the mid-latitudes but not so in the lower latitudes. The same conclusions are still true at 72 hours for both methods (Figures 6.15 and 6.16). Therefore for these types of flows, slow high Burger number regimes then we would have to conclude that the extra terms may not be worth the extra information given the extra work to calculate the extra terms.

The other set of experiments that we performed in this chapter involved a s^h–lursTJ¯y–isfeo^h–l–u^h–Cl–uu–(Figurec–s–s–d–othy–isfhoiffnwhen

equations. The main conclusion for the RV method was that for TC1 types of flows then the effects coming from T_6 in (4.34) could possibly be removed and the ellipticity condition would only be affected slightly. The same was true for the scale analysis for the coefficients in the differential equation.

For TC2 we saw that for the ellipticity condition the extra terms were comparable with the Laplacian operator and should be kept in but also that the B^2 coefficients were the same magnitude as some of the coefficients in $4AC$. This would suggest that the higher order correction is needed here but there was a question of the possibility that the ellipticity condition could be violated for flows that are much faster that the speed of the wave in TC2 but also for heights much higher than those in TC2.

TC3 analysis showed that for flows of this type we should only consider the Laplacian and that the extra terms are small in comparison.

In the PV method's scale analysis for TC1 we see that the Helmholtz term we onlyn–termsˆTD¯–and–m–wTj¯ˆˆTD¯w a

latitudes suggesting that the geostrophic approximation could be enough in the mid-latitudes.

hapter 7

Balanced Variables Experiments

In this chapter we present results from two sets of experiments involving the numerical solutions to (5.1) and (5.2). The first set of experiments involve the solution to (5.1) and (5.2) with $\alpha = 0$ and 1. In these experiments we calculate the solutions to the diagnostic equations considering both a constant and a variable Coriolis parameter. The value that we use for the constant f case is 10^{-4} as an approximation to the value of f in the mid-latitudes. The shallow water equation model that w

testing the variable.

The second set of experiments in

7.1 Description of Experiments

As we mention in the introduction to this chapter we perform experiments to calculate the balanced height increment. We use the numerical approximations described in Section 5.2.2 where the result is a sparse square matrix that has to be inverted to find h'.

For the RV method the left hand side of the discrete version of (5.1) is approximated by (5.26), given $\mathbf{u}'$. This is defined in Section 7.2.2. For the PV method we use the central difference approximations to all the terms in the discrete version of (5.1) as this is the numerator of the first term on the right hand side of (5.2). To calculate the numerical approximation to $\bar{\xi}^c$ we use the central differences described in Section 5.2.2 for all the derivatives of $\bar{u}_g$ and $\bar{v}_g$ in (4.68).

For the constant f experiments we multiply throughout by $a^2 f^2 \cos^2\theta$. This is to remove the errors involved with working with small numbers. The term $\frac{1}{a^3} \approx 10^{-18}$ which is small but also the derivatives of the geostrophic winds are around 10^{-6}. For variable f we multiply throughout by $a^2 f^3 \cos^2\theta$. This is to avoid the singularity at the equator due to $f = 0$ there. We are not including the extra terms that arise from the variable f derivatives for these experiments as this is only a first test. This is also to model more physically the underlying flow. This is a Rossby wave and its propagation is dependent

the PV method compared to the RV method, which is more noticeable than in the other two test cases.

In the second experiment we only consider the constant f case as we are testing the hypothesis that the balanced wind field, which also defines the subspace in the phase space of the shallow water equations, is divergent for constant f.

We calculate $\mathbf{u}^{c\prime}$ through evaluating (4.25) and (4.26) where we calculate the coefficients through the expression that we derive in section 5.2.2. We then calculate the divergence by evaluating (5.27) with $\mathbf{u}^{c\prime}$.

7. Incremental Fields

In this section we introduce the choice of base state and increment of h, u and v fields that are used in the experiments described in Section 7.1.

7.2.1 Base State

To calculate our base states we run the shallow water model described in Section 5.2.1 with the three choices for the Rossby-Haurwitz wave, TC1 - TC3, out to 120 hours and use the output of the height, h and the two wind components, u and v at 72 hours into the run.

As a first test we have chosen to use zonal averages as our base state.

This has the affect of removing certain terms in the equations, specifically $\bar{v}_g, \frac{\partial \bar{u}_g}{\partial \lambda}$ and $\frac{\partial \bar{v}_g}{\partial \lambda}$. This does simplify the problem by eliminating the cross derivative terms in the equation but if we have problems with this simple test case then there may be problems with more complicated base states. We calculate the zonal averages by

$$\bar{h}_i = \frac{1}{} \sum_{j \ 1}^{M} h_{i,j}, \tag{7.1}$$

$$\bar{u}_i = \frac{1}{} \sum_{j \ 1}^{M} u_{i,j}, \tag{7.2}$$

that at these two points there is no balanced part to the height above the zonal average here.

The other reason for this choice is when we try to implement the condition $\frac{\partial h'}{\partial \lambda} = 0$ the resulting matrix for the discrete problem is singular. The problem of modelling the pole in spherical coordinates is a tricky one. There are many mathematical ideas to cope with the pole, [2] and [49], but we shall use the simple Dirichlet condition as the theory for elliptic equations holds, [8], [11] and[16]. When we use the periodicity condition in the θ direction to calculate $\mathbf{u}^{c\prime}$ at the poles, we use the approximation $\frac{\Delta\theta}{4}$ to $\cos\theta$ as described in [29].

7.2.2 Increments

Giv

where $\mathbf{u}' = (u', v')^T$ and ξ is the full relative vorticity.

For equation (5.2) we calculate the PV left hand side using the full height increment (7.4) and evaluate (4.68) through using the central differences approximations described in Section 5.2.2 to the right hand side of (5.1), which equals the first term in (5.2). We use (7.1) for the denominators in (5.2).

7.3 Results I: Balanced Height Increments

We consider the results for each test case separately but we look at the results for both the RV and PV methods with constant and variable f.

The first figure, 7.1, displays the full height increments, h'_f, for the three test cases. The initial condition of the Rossby-Haurwitz wave is a balanced flo f

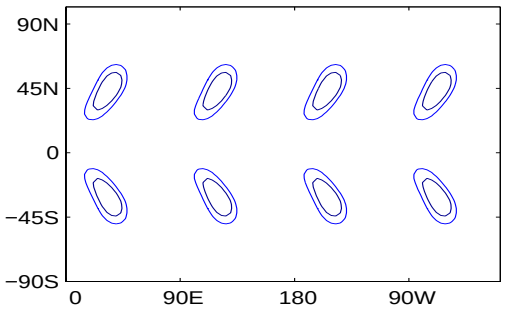
90N
45N
0
−45S
−90S
0
90E
180
90W

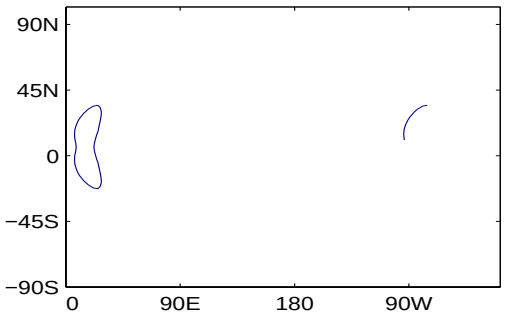
90N
45N
0
−45S
−90S
0
90E
180
90W

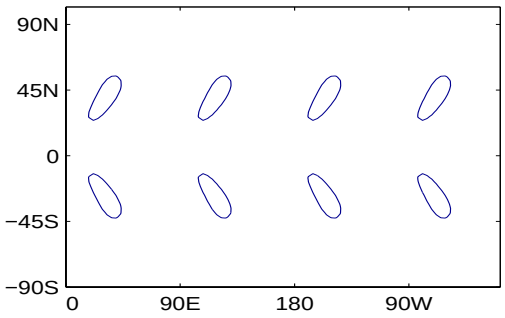
90N
45N
0
−45S
−90S
0
90E
180
90W

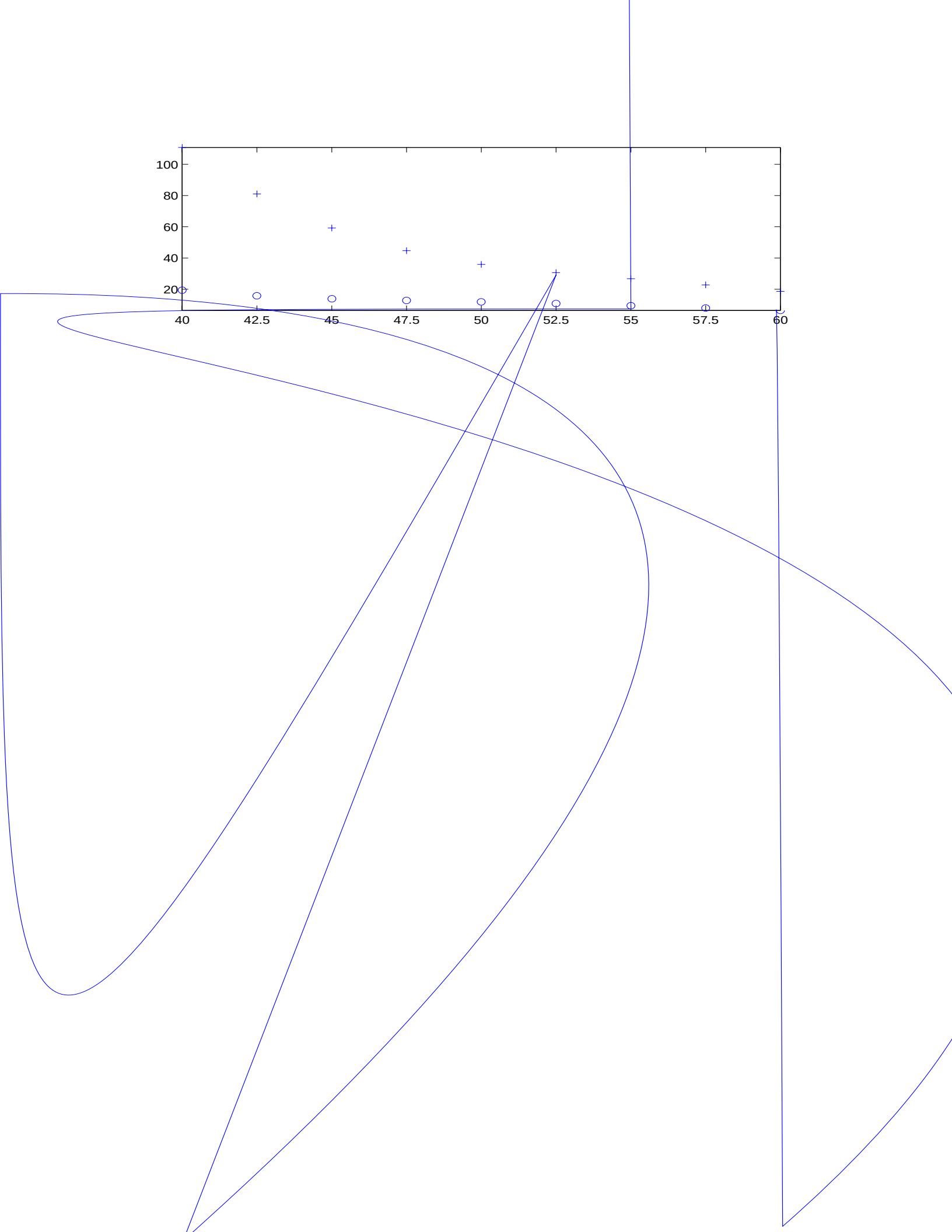
100
80
60
40
20
40
42.5
45
47.5
50
52.5
55
57.5
60

norm of the results for constant f from the PV method we see that the norm for this approximation is smaller than the variable f from the RV method.

For TC2 (see Figure 7.5), we do not have a tilt in the increment that is present in TC1, but the wave from test case two is travelling faster than the wave from test case one also the full height field from test case two grows substantially as we enter the lower latitudes. Although we have removed the $\bar{v}_g$ component from (5.2) and (4.55) along with $\bar{u}_{g\lambda}$ and $\bar{v}_{g\lambda}$ there are still large increases in the height field in the θ direction which could cause an effect on the ellipticity conditions. We do not see that here, as we have a solution that appears to be sensible, but we do again see that with a constant f there does appear to be an effect on the solutions with the under modelling near the equator feeding back into the mid-latitudes. We can see this with the left hand plots in Figure 7.5 where we have the circular formation in the mid-latitudes, (Upper right plot in Figure 7.1), drawn into the equatorial region.

An interesting feature of the constant f plots for the RV method with $\alpha = 1$ is that the circular formation for the full height increment, (top right plot in Figure 7.1), appears –see.–b–e–enb–f–orurttiallyo–t–hehnf

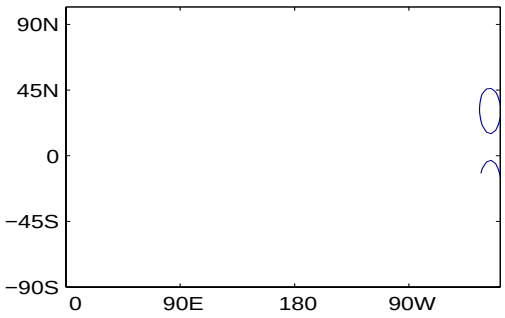
90N
45N
0
−45S
−90S
0
90E
180
90W

for TC1 and as such the differences are on a different scale due to the speed and growth in the wave's height.

For the RV method we see that Figure 7.7 would indicate differently the closeness of the solutions with a variable f

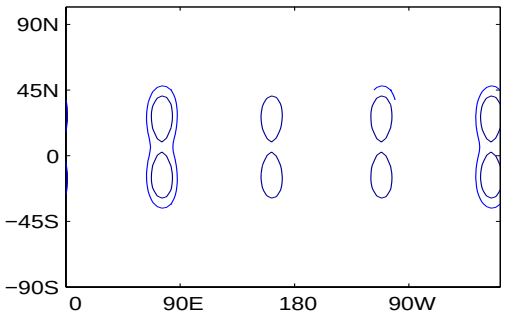
90N
45N
0
−45S
−90S
0
90E
180
90W

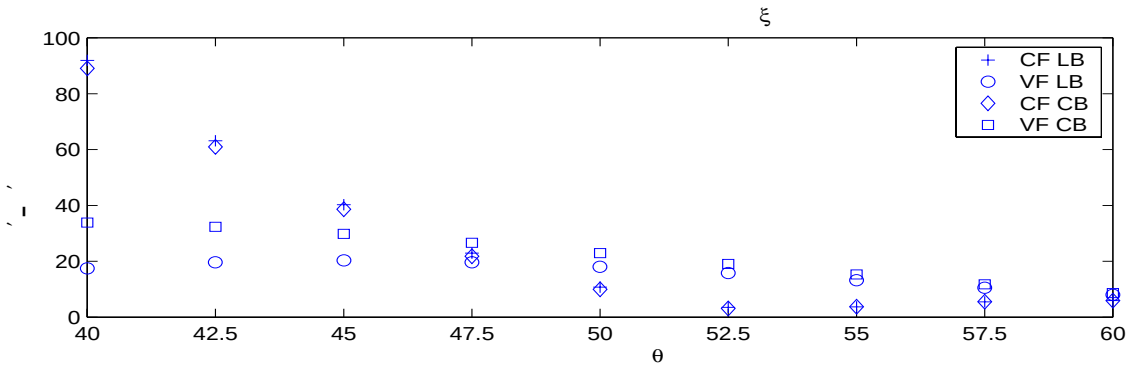
ξ
100
80
60
40
20
0
40
42.5
45
47.5
50
52.5
55
57.5
60
θ
CF LB
VF LB
CF CB
VF CB

We consider each test case in turn. As we have seen from the results in Section 7.3, when we use a constant f then the consequences are quite severe for certain test cases. This has an effect on the calculations of $\mathbf{u}^{c\prime}$ due to $\mathbf{u}'_g$ being dependent on the derivatives of h', (4.22).

Before we show the results for the divew–tˆn robeingeindonnt ew–wTf−−–fiTj¯Tˆ–esthe–90ˆTf¯

for the RV and PV method. However, another feature is the fact that the divergence of the balanced wind field is out of phase with the full divergence. We would not expect the whole divergence to be balanced but we have to recall that the heights for this test case when we use a constant f were severely different from the full height field even in the mid-latitudes. This would affect the calculations of $\mathbf{u}^{c\prime}$ as we mentioned earlier in this section. This would cause some of the displacement of the divergence due to the maximum heights being a lot larger than those of the full height increment.

If we now consider TC2 results, (Figures 7.14 and 7.15) then the plots corresponding to the divergence of the geostrophic winds for TC2 are again only showing random machine noise and are 10^{-14} smaller than the results for the higher order balanced wind and have no structure.

Unlike for TC1 the divergence is in phase with the full divergence but for this test case we have the balanced increments divergence larger than that of the full increments. If we recall the size of the height increment for this test case when we use a constant f then we see that there were large differences between the full height increment and the balanced increment even in the mid-latitudes (Figure 7.7).

Therefore, as we have mentioned in the summary of the results for the divergence for TC1, the height field is used to calculate $\mathbf{u}^{c\prime}$ and if this is incorrect then the divergence will be affected as well.

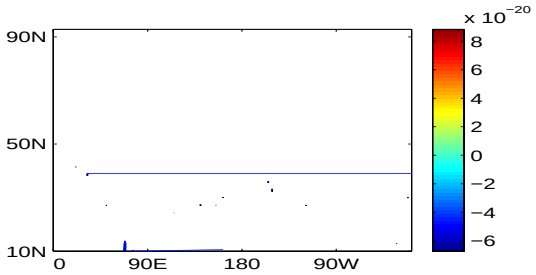
90N
50N
10N
0
90E
180
90W
x 10^−20
8
6
4
2
0
−2
−4
−6

Another feature is the difference between the divergence when $\alpha = 1$ for the RV and PV method. There appears to be a slanting of the divergence in the result for the RV method compared to the result for the equivalent in the PV method. This slanting effect is in the higher latitudes in both the Northern and Southern hemisphere.

If we now consider the final test case, TC3, then we again have the geostrophic winds being divergence free for constant f.

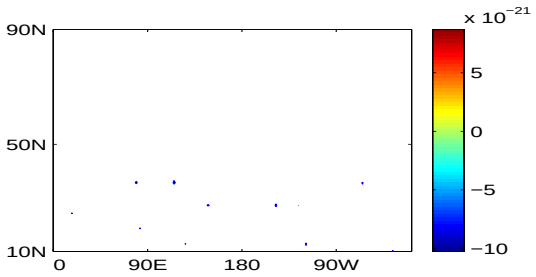

approximation are connected. Hence the incorrect modelling in the equatorial regions is fed back to the mid-latitudes through the matrix inversion.

This then raises the problem of dealing with the $\frac{1}{f}$ term at the equator. We must remember that the underlying theory for this balanced subspace of the full phase space assumes that the Rossby number is small, [31], [41].

When we did introduce a variable f there was a noticeable improvement in the approximations. If we consider the results for TC1 in the mid-latitudes (Figure 7.4), then we see that the introduction of the PV instead of RV reduces $\|h'_f - h'\|$, consistent with [57].

The surprising result for TC1 is the test case's divergence for the balanced increment is the only one to be smaller than the full increment. This test case also had the smallest norm of the difference between the full height increment and the balanced increment.

For TC2 we had the variable f not improving the solution very much and for the most part, in the mid-latitudes (Figure 7.7) the RV and PV methods performed better with $\alpha = 0$ than with $\alpha = 1$. TC2 is the most extreme of the three and in the scale analysis we saw that the B^2 terms were of similar magnitude to $4AC$. The choice of base state that we use for these experiments makes the B^2 term zero, which may have affected the solution more than in the test case.

terms would not affect the solution too much, especially in the mid-latitudes. We also see this in Figure 7.10 where we have for most of the mid-latitudes, the symbols representing the $\alpha = 0$ and $\alpha = 1$ almost always together.

In summary: We have to say that the PV method does improve the approximations to the balanced flow for low Burger number regimes, (TC1). We also see that the effect of constant and variable f is the most severe for this type of flow. For flows similar to TC2 the use of a zonal average does not appeardoannFTJ^{-}ˆˆTD^{-}ˆ–z–ˆdol

hapter 8

onclusions and Further Work

In this chapter we expand on the conclusion in Chapters 6 and 7 and then suggest some extension to this w

given either an increment to the relative vorticity or the linearised potential vorticity. If this new method is to be considered as a replacement for the current balanced control variable then we have to see if there is any benefit in the calculation of the extra terms and the extra storage required to calculate the numerical solutions to the elliptic equations (5.1) or (5.2) with $\alpha = 1$.

In Section 6.3 we compare the ellipticity condition for the three test cases at both the initial time and at 72 hrs for both the RV and PV method when $\alpha = 1$ to see if the Laplacian's ellipticity condition was the dominant feature.

For TC1 with the R

The scale analysis for the ellipticity condition for this method would conclude that the extra terms are a small factor compared to the Laplacian, (Tables 6.5 and 6.6), in the mid-latitudes with a global constant f. When considering the terms in the differential equation, (Table 6.7), then we saw that the Helmholtz part of the equation dominated the remaining terms and therefore must be included. This would suggest that the PV method should be used for this type of flow. This is consistent with the findings in [57] but with the PV defined in a different manner.

From the numerical results to (5.1) and (5.2) for TC1, (Figures 7.2 and 7.3) then for a constant f the results were not too good with the RV method with either $\alpha = 0$ or 1 but with the PV method we saw major improvements especially in the mid-latitudes, (Figure 7.4) even for constant f.

We saw a cut off when we use a variable f with $\alpha = 1$ in both the RV and PV methods where the asymptotic expansion is no longer valid as the Rossby number is tending to infinity in the equatorial regions. The choice of a zonal average with this test case does not seem to affect the results too severely but the scale analysis suggested that the extra terms may only be a small consequence at 72 hrs.

The balanced wind increment associated with this height increment was divergent but out of phase with the full divergence. (Figures 7.12 and 7.13).

TC2 appears to be the type of flow that requires the extra terms. This

suggest that with a constant f there are still problems with the bad modelling of the flow but also the removal of the zonal averaged relative vorticity could be too severe for this flow as well.

The balanced wind field with this test case using a constant f was div

economical to use the RV method.

Although these conclusions are for the Burger number we recall the definition given for the number

$$B_u \equiv \frac{\sqrt{gh}}{fL}, \tag{8.1}$$

we see that this is a ratio between the height and the horizontal length scale. There are other factors that have to also be considered. The expansion for the balance wind field is dependent on the Rossby number

$$R_0 \equiv \frac{V_H}{2\Omega L_H}, \tag{8.2}$$

being small. This number is dependent on the ratio of the horizontal wind speed scale and the length scale. Therefore we also have to consider the scale of the winds associated with the flow regime.

We also have to be aware of large changes in the height profile over short distances. This affect the geostrophic winds which are the gradients of the height field with respect to the two horizontal coordinate directions (4.16). These are some of the coefficients in the ellipticity condition but also their gradients as well.

Therefore the Burger number is a good first stage test to see if the flow requires the extra terms but we must also consider the speed of the winds associated with the flow to confirm that the Rossby number is small but also the change in the height over short distances to ensure that the geostrophic

component is small enough to not violate the ellipticity condition.

8. Further ork

The choice of base state was a simple first choice to test the numerics that we use to calculate the numerical solutions to the elliptic pde that arose from the balanced subspace in the shallow water equation's full phase space.

Therefore there are many other choices of base states that could be used in the linearisation. One possible choice is to perturb the parameters that

When we were deciding on the base state we considered perturbing the ω parameter by 10% for the two choices used. Due to the properties of the Met Office's shallow water code, [28], when we implemented this to generate

The main area of development for this work would be to introduce the balanced wind field into a limited area model, (LAM). There are plans to introduce a LAM at the Met Office for the North Atlantic this autumn. Constraining the balanced wind field to the mid-latitudes would be a logical

stsw

the constant Coriolis case where we possibly had errors from the equator feeding back to the mid-latitudes, (Section 7.3).

A further suggestion for more work would be to develop a diagnostic test for the balanced height and the control variables described in Section 4.4. A possible means to do this would be to calculate the divergence tendencies for the variables using the technique described in [57].

The benefit of this test w

boundary conditions. This functional is given by

$$I \equiv \int_v \sum_i \alpha_i^2 \left(f_{0t} - f_i\right)^2 \mathrm{d}V. \tag{8.4}$$

Sasaki requires this functional to be minimised and so applies a variation to obtain

$$\delta I \equiv \delta \int_v \sum_i \alpha_i^2 \left(f_{0t} - f_i\right)^2 \mathrm{d}V. \tag{8.5}$$

Sasaki then applies standard calculus of variation techniques, [9], to find the minimum of the functional, (8.4). He introduces the following as the model variables, u, v ϕ and T, where ϕ is the geopotential and T is the absolute temperature.

Next Sasaki substitutes the geostrophic winds in place of the full wind fields and then forms the difference between the full fields and the observations. This then gives the sum of squares as

$$\varepsilon^2 \equiv \alpha_1^2 u'^2 + \alpha_2^1 v'^2 + \alpha_2^2 \phi'^2 + \alpha_3^2 T'^2, \tag{8.6}$$

where the increments are given by

$$u' = -\frac{1}{f}\frac{\partial \phi'}{\partial y} - u_o - \frac{1}{f}\frac{\partial \phi_o}{\partial y}, \tag{8.7}$$

$$v' = \frac{1}{f}\frac{\partial \phi'}{\partial x} - v_o + \frac{1}{f}\frac{\partial \phi_o}{\partial x}, \tag{8.8}$$

$$\phi' = \phi - \phi_0, \tag{8.9}$$

$$T' = \frac{\partial \phi'}{\partial p^*} - T_o + \frac{\partial \phi_o}{\partial p^*}, \tag{8.10}$$

where p^* represents the vertical coordinate system

The resulting Euler equation that minimises (8.4) given (8.6) is

$$\nabla^2\phi' - \left(\frac{\alpha_2}{\alpha_1}f\right)^2 = f\xi_0 - \nabla^2\phi_0, \tag{8.11}$$

where

$$\xi_0 \equiv \frac{\partial v_0}{\partial x} - \frac{\partial u_0}{\partial y}.$$

Sasaki interprets the results of (8.11) as follows: if the right hand side is zero then the modified values are equal to the observed quantities. These observed quantities could be used in n

these variables with a data assimilation scheme yet but do see this as an important part of the development of these variables.

Bibliography

[1] K. E. Atkinson. *An Introduction to Numerical Analysis*. Wileys, 1989.

[2] S. R. M. Barros. Multigrid Methods for Two- and Three-Dimensional Poisson-Type Equations on the Sphere. *Journal of Computational Physics*, **92**:313–348, 1991.

[3] G. K. Batchelor. *An Introduction to Fluid ynamics*. Cambridge University Press, 1967.

[4] G. Browning, A. Kasahara, and H. Kreiss. Initialization of the Primitive equations by the Bounded Derivative Method. *Journal of Atmospheric Science*, **37**:1424–36, 1979.

[5] A. P. Burger. Scale Consideration of Planetary Motions of the Atmosphere. *A uarterly Journal of Geophysics*, **10**:195–205, 1958.

[6] A. P. Burger. On the Non-Existence of Critical Wavelength in a Continuous Baroclinic Stability Problem. *Journal of Atmospheric Science*, **19**:30–38, 1962.

[7] J. Charney. The use of the Primitive Equations of Motion of the Atmosphere. *Tellus*, **7**:22–26, 1955.

[8] C. R. Chester. *Techniques in Partial ifferential Equations.* McGraw-Hill Book Company, 1971.

[9] J. C. Clegg. *Calculus of ariation.* Oliver and Boyd Ltd, 1968.

[10] R. Courant and D. Hilbert. *Methods of Mathematical Physics, olume ne.* Interscience Publishers, Inc, 1953.

[11] R. Courant and D. Hilbert. *Methods of Mathematical Physics, olume Two: Partial ifferential Equations.* Interscience Publishers, Inc, 1962.

[12] W. Cox. *ector Calculus.* Arnold, 1998.

[13] M. J. P. Cullen and R. J. Purser. An extended Lagrangian Theory of Semi-geostrophic Frontogenesis. *Journal of Atmospheric Sciences*, **41**:1477–1497, 1984.

[14] R. Daley. *Atmospheric ata Analysis.* Cambridge University Press, 1991.

[15] G. Desroziers and J. P. Lafore. A Co-ordinate Transformation for Objective Frontal Analysis. *Monthly Weather Review*, **121**:1531–1553, 1993.

[16] P. R. Garabedian. *Partial ifferential Equations*. John Wiley and Sons, 1967.

[17] G. J. Haltiner and R. T. Williams. *Numerical Prediction and ynamic Metrorology*. John Wiley and Sons, 1980.

[18] B. Haurwitz. The Motion of Atmospheric Disturbances on the Spherical Earth. *Journal of Marine Research*, **3**:254–267, 1940.

[19] J. R. Holton. *An Introduction to ynamic Meteorology*. Academic Press, 1992.

[20] B. J. Hoskins. Stability of the Rossby-Haurwitz Wave. *uarterly Journal of the Royal Meteorological Society*, **99**:723–745, 1973.

[21] B. J. Hoskins. The Geostrophic Momentum Approximation and the Semigeostrophic Equations. *Journal of Atmospheric Sciences*, **32**:233–242, 1975.

[22] D. D. Houghton. Derivation of the Elliptic Condition for the Balance Equation in Spherical Coordinates. *Journal of Atmospheric Sciences*, **25**:927–928, 1968.

[23] A. Iserles. *A First Course in the Numerical Analysis of ifferential Equations*

[30] M. E. McIntyre and I. Roulstone. Hamiltonian balanced models: Constrained, slow manifolds and velocity-splitting. Technical report, Met. Office, U.K., 1996. Forecasting Research Scientific Paper **41**.

[31] M. E. McIntyre and I. Roulstone. Are there higher-accuracy analogues of semi-geostrophic theory? *Newton Institute: Large-Scale Atmosphere-cean ynamics*, **2**: Geometric Methods and Models:301–364, 2002.

[32] K. W. Morton and D. F. Mayers. *Numerical Solution of Partial iffer-ential Equations*. Cambridge University Press, 1996.

[33] J. Paegle and J. N. Paegle. An Efficient and Accurate Approximation to the Balance Wind with Application to Non-Elliptic Data. *Monthly Weather Review*, **102**:838–846, 1974.

[34] J. Pedlosky. *Geophysical Fluid ynamics*. Springer-Valger, 1979.

[35] N. Phillips. On the Problem of the Initial Data for the Primitive Equations. *Tellus*, **12**:121–126, 1960.

[36] C. G. Rossby. Planetary Flow Patterns in the Atmosphere. *uarterly Journal of the Royal Meteorological Society*, **66**:68–87, 1940. Supplement.

[37] I. Roulstone and M. J. Sewell. Potential Vorticities in Semi-geostrophic Theory. *uarterly Journal of the Royal Meteorological Society*, **122**:983–992, 1996.

[38] R. Salmon. Practical use of the Hamilton's principle. *Journal of Fluid Mechanics*, **132**:431–444, 1983.

[39] R. Salmon. New Equations for the Nearly Geostrophic Flow. *Journal of Fluid Mechanics*, **153**:461–477, 1985.

[40] R. Salmon. Hamiltonian Fluid Dynamics. *Annual Review of Fluid y-namics*, **20**:225–256, 1988.

[41] R. Salmon. Semi-Geostrophic Theory as a Dirac-Bracket Projection. *Journal of Fluid Mechanics*, **196**:345–358, 1988.

[42] R. Salmon. *Lectures on Geophysical Fluid ynamics*. Oxford University Press, 1998.

[43] Y. Sasaki. An Objective Analysis Based on the Variational Method. *Journal of the Meteorological Society Japan*, **36**:77–88, 1958.

[44] Y. Sasaki. Some Basic Formalisms in Numerical Variational Analysis. *Monthly Weather Review*, **36**:875–883, 1970.

[45] G. J. Shutts. Planetary Semigeostrophic Equations Derived from Hamilton's Principle. *Journal of Fluid Mechanics*, **208**:545–573, 1989.

[46] G. D. Smith. *Numerical Solution of Partial ifferential Equations.* Oxford University Press, 3rd Edition, 1999.

[47] C. Snyder, W. C. Skamarock, and R. Rotunno. A Comparison of Primitive-Equation and Semigeostrophic Simulations of Baroclinic Waves. *Journal of Atmospheric Sciences*, **48**:2179–2194, 1991.

[48] M. R. Spiegel. *ector Analysis, Schaum's utline.* McGraw Hill, 1959.

[49] P. N. Swarztrauber. The Direct Solution of the Discrete Poisson Equation on the Surface of the Sphere. *Journal of Computational Physics,*, **15**:46–54, 1974.

[50] J. Thurburn and Y Li. Numerical Simulations of the Rossby-Haurwitz Waves. *Tellus*, **52A**:181–189, 2000.

[51] R. S. Varga. *Matrix Iterative Analysis.* Prentice Hill Inc, 1962.

[52] G. Veitch and M. H. Mawson. A Comparison of Inertial Stability Conditions in the Planetary Semi-Geostrophic and Quasi-Equilibrium Models. Technical report, **60**, 2001. Forecasting Research Division, Met. Office, U.K.

Appendix A: Spherical Vector Operator

Spherical Unit Vectors

When transforming from Cartesian coordinates to spherical coordinates the direction in which the unit vectors are pointing changes. In spherical coordinates there is a local approximation through a tangential plane relative to the spherical surface, (see figure 8.1).

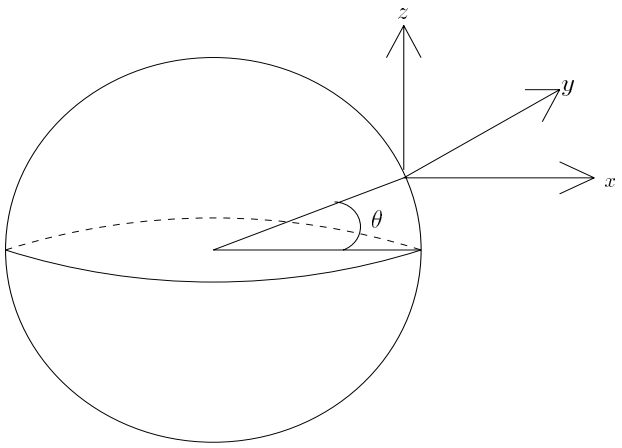

$$\begin{aligned}
\frac{\partial \mathbf{j}}{\partial r} &= 0, \quad \frac{\partial \mathbf{j}}{\partial \theta} = -\mathbf{k}, \quad \frac{\partial \mathbf{j}}{\partial \lambda} = -\sin\theta \mathbf{i}, \\
\frac{\partial \mathbf{k}}{\partial r} &= 0, \quad \frac{\partial \mathbf{k}}{\partial \theta} = \mathbf{j}, \quad \frac{\partial \mathbf{k}}{\partial \lambda} = \cos\theta \mathbf{i}.
\end{aligned}$$

The full derivation of these expression is found in [3]. As we are using a 2-D framework for the SWE then we have a constant radial distance and hence no change along $\mathbf{k}$. This then makes all the terms in the derivtives that contain $\mathbf{k}$ zero. The remaining terms are

$$\frac{\partial \mathbf{i}}{\partial \lambda} = \sin\theta \mathbf{j},$$

i4TiofslTf-kiofkhimrseTD-noTj-po--B:DT-r

The next operator is the div

Appendix B: Geostrophic ind Identities

In Chapter 4 we use three different identities involving the θ derivatives of vg and here in this appendix we will show the derivation to these results. We begin with $\frac{\partial v_g}{\partial \theta}$

$$\frac{\partial v_g}{\partial \theta} = \frac{\partial}{\partial \theta}\left(\frac{g}{af\cos\theta}\frac{\partial h}{\partial \lambda}\right. = \overbrace{\frac{g\tan\theta}{af\cos\theta}\frac{\partial h}{\partial \lambda}}^{T_1} + \overbrace{\frac{g}{af\cos\theta}\frac{\partial^2 h}{\partial\theta\partial\lambda}}^{T_2} + \overbrace{\frac{g}{a\cos\theta}\frac{\partial h}{\partial\lambda}\frac{\partial}{\partial\theta}\left(\frac{1}{f}\right.}^{T_3}.$$

We can see that T_1 is simply $\tan\theta v_g$, T_2 is $-\frac{1}{\cos\theta}\frac{\partial u_g}{\partial\lambda}$, the third term, T_3 is almost v_g but we are missing the f^{-1} term so then this term is $fv_g\Gamma_1$, where Γ_1 is as defined in Chapter 4. We now consider the second order derivatives. We start with

$$\frac{\partial^2 v_g}{\partial\theta\partial\lambda} = \frac{\partial}{\partial\theta}\left(\frac{g}{af\cos\theta}\frac{\partial^2 h}{\partial\lambda^2}\right. = \overbrace{\frac{g\tan\theta}{af\cos\theta}\frac{\partial^2 h}{\partial\lambda^2}}^{T_1} + \overbrace{\frac{g}{af\cos\theta}\frac{\partial^3 h}{\partial\theta\partial\lambda^2}}^{T_2} + \overbrace{\frac{g}{a\cos\theta}\frac{\partial^2 h}{\partial\lambda^2}\frac{\partial}{\partial\theta}\left(\frac{1}{f}\right.}^{T_3}.$$

This now gives for T_1 here $\tan\theta\frac{\partial v_g}{\partial\lambda}$, T_2 is $-\frac{1}{\cos\theta}\frac{\partial^2 u_g}{\partial\lambda^2}$ and T_3 is $f\frac{\partial v_g}{\partial\lambda}$. The final identitiy is a little harder to derive but it starts from

$$\begin{aligned}\frac{\partial^2 v_g}{\partial\theta^2} &= \frac{\partial}{\partial\theta}\left(\frac{\partial}{\partial\theta}\left(\frac{g}{af\cos\theta}\frac{\partial h}{\partial\lambda}\right.\right.\\ &= \frac{\partial}{\partial\theta}\left(\frac{g\tan\theta}{af\cos\theta}\frac{\partial h}{\partial\lambda} + \frac{g}{af\cos\theta}\frac{\partial^2 h}{\partial\theta\partial\lambda} + \frac{g}{a\cos\theta}\frac{\partial h}{\partial\lambda}\frac{\partial}{\partial\theta}\left(\frac{1}{f}\right.\right.\end{aligned}$$

which gives

$$\frac{\partial^2 v_g}{\partial\theta^2} = \overbrace{\left(\frac{g}{af\cos^3\theta} + \frac{g\tan^2\theta}{af\cos\theta}\right.\frac{\partial h}{\partial\lambda}}^{T_1} + \overbrace{\frac{2g\tan\theta}{af\cos\theta}\frac{\partial^2 h}{\partial\theta\partial\lambda}}^{T_2} + \overbrace{\frac{g}{fa\cos\theta}\frac{\partial^3 h}{\partial\theta^2\partial\lambda}}^{T_3}$$

$$+ \underbrace{\frac{2g\tan\theta}{a\cos\theta}\frac{\partial h}{\partial\lambda}\frac{\partial}{\partial\theta}\left(\frac{1}{f}\right.}_{T_4} + \underbrace{\frac{2g}{a\cos\theta}\frac{\partial^2 h}{\partial\theta\partial\lambda}\frac{\partial}{\partial\theta}\left(\frac{1}{f}\right.}_{T_5} + \underbrace{\frac{g}{a\cos\theta}\frac{\partial^2}{\partial\theta^2}\left(\frac{1}{f}\right.}_{T_6}.$$

Therefore T_1 becomes $(2\tan^2\theta + 1)\, v_g$ where we have used the trig identity, $\sec^2\theta = \tan^2\theta + 1$. The second term, T_2 is $-\frac{\tan\theta}{\cos\theta}\frac{\partial u_g}{\partial\lambda}$, where T_3 is $-\frac{1}{\cos\theta}\frac{\partial^2 u_g}{\partial\lambda\partial\theta}$. The fourth term, T_4 is $2f\tan\theta v_g\Gamma_1$ and the fifth term, T_5, is $-\frac{2}{\cos\theta}\frac{\partial u_g}{\partial\lambda}\Gamma_1$. The final term, T_6 is $f v_g\Gamma_2$.

Appendix C: Rossby-Haurwitz ave's Derivatives

In this appendix we list the derivatives for the A, B and C terms in the definition of the Rossby-Haurwitz wave with respect to θ.

We begin with the A term. This derivative is

$$\frac{\partial A}{\partial \theta} = -\omega\,(2\Omega + \omega$$

Therefore we have

$$\frac{\partial A_1}{\partial \theta} = -\omega\left(2\Omega+\omega\right)\left(\cos^2\theta-\sin^2\theta\right),$$

∂A